

Review

Advances in the Fabrication and Magnetic Properties of Heusler Alloy Glass-Coated Microwires with High Curie Temperature

Mohamed Salaheldeen ^{1,2,3,4,*} , Valentina Zhukova ^{1,2,4} , Juan Maria Blanco ^{1,2}, Julian Gonzalez ^{1,2} and Arcady Zhukov ^{1,2,4,5,*} 

¹ Department of Polymers and Advanced Materials, Faculty of Chemistry, University of the Basque Country, UPV/EHU, 20018 San Sebastián, Spain; valentina.zhukova@ehu.eus (V.Z.); juanmaria.blanco@ehu.eus (J.M.B.); julianmaria.gonzalez@ehu.eus (J.G.)

² Department of Applied Physics I, EIG, University of the Basque Country, UPV/EHU, 20018 San Sebastián, Spain

³ Physics Department, Faculty of Science, Sohag University, Sohag 82524, Egypt

⁴ EHU Quantum Center, University of the Basque Country, UPV/EHU, 20018 San Sebastián, Spain

⁵ IKERBASQUE, Basque Foundation for Science, 48011 Bilbao, Spain

* Correspondence: mohamed.salaheldeenmohamed@ehu.eus (M.S.); arkadi.joukov@ehu.eus (A.Z.)

Abstract

This review article provides an in-depth analysis of recent advancements in the fabrication, structural characterization, and magnetic properties of Heusler alloy glass-coated microwires, focusing on Co_2FeSi alloys. These microwires exhibit unique thermal stability, high Curie temperatures, and tunable magnetic properties, making them suitable for a wide range of applications in spintronics, magnetic sensing, and biomedical engineering. The review emphasizes the influence of geometric parameters, annealing conditions, and compositional variations on the microstructure and magnetic behavior of these materials. Detailed discussions on the Taylor–Ulitsky fabrication technique, X-ray diffraction (XRD) analysis, and scanning electron microscopy (SEM) provide insights into the structural properties of the microwires. The magnetic properties, including room-temperature behavior, temperature dependence, and the effects of annealing, are thoroughly examined. The potential applications of these microwires in advanced spintronic devices, magnetic sensors, and biomedical technologies are explored. The review concludes with future research directions, highlighting the potential for further advancements in the field of Heusler alloy microwires.

Keywords: Heusler alloys; glass-coated microwires; magnetic properties; spintronics; annealing effects



Academic Editors: Zhongwu Liu, Hongya Yu and Youlin Huang

Received: 11 April 2025

Revised: 20 June 2025

Accepted: 23 June 2025

Published: 27 June 2025

Citation: Salaheldeen, M.; Zhukova, V.; Blanco, J.M.; Gonzalez, J.; Zhukov, A. Advances in the Fabrication and Magnetic Properties of Heusler Alloy Glass-Coated Microwires with High Curie Temperature. *Metals* **2025**, *15*, 718. <https://doi.org/10.3390/met15070718>

Copyright: © 2025 by the authors. Licensee MDPI, Basel, Switzerland. This article is an open access article distributed under the terms and conditions of the Creative Commons Attribution (CC BY) license (<https://creativecommons.org/licenses/by/4.0/>).

1. Introduction

In recent years, ferromagnetic materials have attracted growing interest owing to various applications in magnetic sensors [1–5], magnetic refrigeration [6–8], microwave engineering [9,10], and spintronics [10–32] because of their distinctive magnetic properties, which allow for the control and manipulation of spin currents. Among various ferromagnetic materials, micro/nano-structured materials have shown great potential for improving the performance of spintronic devices and communication engineering [10–32]. Spintronics is one of the most promising multidisciplinary research fields, facilitating the development of next-generation nano- and microdevices that offer enhanced processing and memory

capabilities while using less power [33–56]. To meet various essential criteria, such as high spin polarization and high Curie temperature (T_c), a new generation of multifunctional materials needs to be developed. Heusler alloys based on Co_2YZ are notable for their high spin polarization (P) and potential half-metallicity (P 100%). However, both theoretical and experimental studies indicate that spin polarization is highly sensitive to structural instability. The L2_1 crystalline phase provides the highest structural order, essential for achieving the desired spin-polarization levels. While the exchange of atoms at the Y–Z positions (B2 disorder) has a minimal impact on spin polarization, disorders involving X–Y or X–Y–Z positions (D03 or A2) can significantly reduce it. Additionally, these Heusler alloys have complex crystalline structures that require very high temperatures (typically over 1000 K in bulk form and over 650 K in thin-film form) for proper crystalline ordering. Consequently, a major challenge in producing X_2YZ full-Heusler low-dimensional materials is achieving the chemically ordered L2_1 phase, as the superior properties of Co_2 -based Heusler compounds are generally expected in this phase (see Figure 1).

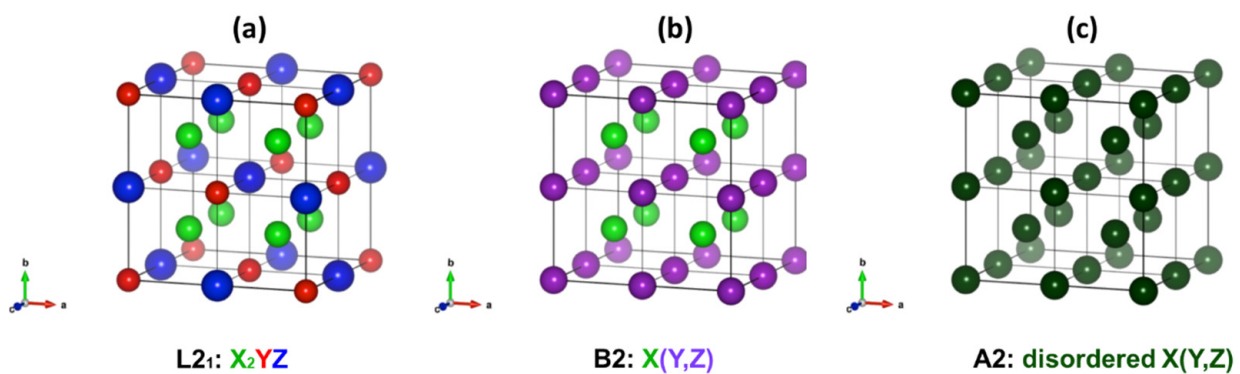


Figure 1. Crystal structures of (a) L2_1 phase and typical disordered phases in Heusler alloys: (b) B2 and (c) A2. B2 phase is disordered between Y and Z but ordered between X and (Y, Z). A2 phase is a completely disordered (random) structure (bcc structure). Unit cells of B2 and A2 are shown by thicker lines in (b,c). Figures were Adapted from Ref. [57].

Heusler compounds are particularly well-suited for spintronic and magnetoelectronic applications [31,40]. Their advantages include excellent lattice matching with common substrates, T_c above room temperature, and the potential to achieve nearly 100% spin polarization near the Fermi level [40]. Co-based Heusler compounds are highly promising for multifunctional applications due to their low magnetic damping coefficients, high Curie temperature ($T_c > 1200$ K), adjustable band structure, and high magnetic moment. Additionally, these alloys exhibit remarkable and unusual physical properties both above and below room temperature, attributed to the significant Berry curvature associated with their band structure.

The aforementioned evidence highlights why Co-based full-Heusler alloys have garnered significant interest within the scientific community [58–63]. Consequently, these alloys are extensively studied in various forms, including nanoparticles, thin films, and nano/microwires [63–84]. However, it is important to note that producing Heusler alloy nanoparticles and thin films presents several challenges for practical applications. These challenges include the high cost of fabrication methods, chemical composition inhomogeneity, time consumption, and susceptibility to oxidation [52–55,72]. Additionally, the diffusion of substrate atoms into the films often leads to atomic disorder and phase separations, which are commonly observed [82,84]. The mismatch between the lattice structures of the alloy and the substrate further complicates fabrication. Moreover, to achieve the necessary structural ordering, Heusler alloys produced by arc melting or thin-film deposition require prolonged annealing at high temperatures [60,82]. The pri-

mary method for producing Heusler alloys is arc melting, followed by additional thermal treatment [40,55,60,63]. This technique allows for the fabrication of Heusler alloys in bulk form. However, miniaturization has been explored as an alternative strategy to enhance the properties of these alloys [84]. Reducing the dimensions of Heusler alloys can significantly improve their performance. For example, in magnetic cooling applications, decreasing the size of these alloys can increase the surface-to-volume ratio, thereby substantially enhancing the heat-exchange rate.

Since the 1960s, rapid melt quenching has been widely recognized by scientists as an effective method for producing innovative materials with diverse morphological characteristics, with either amorphous and nano/microcrystalline structures or metastable phases with reduced dimensions [85–89]. This technique enables the fabrication of alloys with precise chemical compositions through rapid solidification. Such materials with amorphous structure can present enhanced mechanical, magnetic, and corrosion properties [89–95]. Rapid melt quenching methods have been refined to produce a range of materials, such as ribbons, wires, flakes, microwires, and composite microwires. The final structure of these materials is significantly influenced by factors such as the phase diagram of the selected alloy, quenching conditions, and the geometry of the produced materials.

As previously noted, crystalline materials obtained through rapid quenching generally exhibit inferior mechanical and corrosion properties compared to their amorphous counterparts [89,96–99]. However, rapidly quenched crystalline materials can possess other desirable properties for various applications, such as Giant magnetoresistance or magnetocaloric effect [86,88]. Additionally, the challenge of miniaturizing rapidly quenched materials has become a key focus for numerous applications. As a result, considerable attention has been directed in recent years toward developing preparation methods capable of meeting these requirements.

The Taylor–Ulitsky method has become a highly promising technique for miniaturizing rapidly quenched materials while simultaneously improving their magnetic, corrosion, and mechanical properties [89,92–113]. This technique allows the production of thin metallic microwires, with metallic nucleus diameters ranging from 0.02 to 100 μm (with a difference of almost 4 orders of magnitude), coated by insulating glass [104,109]. The resulting glass-coated microwires, which may possess either amorphous or nanocrystalline structures, exhibit excellent magnetic softness. In addition, the thin glass coating imparts several advantages, such as enhanced mechanical strength, corrosion resistance, improved adhesion to polymer matrices, and biocompatibility [89,97]. Several successful efforts have been made to fabricate such wires using the in-rotating-water technique [102] or by producing glass-coated microwires from Heusler alloys via the Taylor–Ulitsky method [78,80,88,89,92,104–108]. A key feature of the Taylor–Ulitsky technique is its ability to simultaneously solidify metallic alloy and coat them with insulating glass [89,95,96,113–127]. Such process creates internal stresses due to the mismatch in the thermal expansion coefficients between the glass and the metallic alloy [95,100]. The magnitude of these internal stresses, σ_i , is related to the ratio (ρ) between the diameter of the metallic nucleus, d_{metal} and the total, D_{total} diameters. Therefore, these internal stresses can be controlled by adjusting the ρ -ratio [95,100,113,115].

This review article focuses on the fabrication, structural characterization, and magnetic properties of Heusler alloy glass-coated microwires, specifically Co_2FeSi alloys. These microwires exhibit remarkable thermal stability, high Curie temperatures, and tunable magnetic properties, which are influenced by factors such as geometric parameters, annealing conditions, and compositional variations.

2. Materials and Methods

The experimental conditions for synthesizing bulk and glass-coated microwires of Co_2FeSi have been comprehensively detailed in previous studies [75,78]. The primary objective of this study is to fabricate these samples with different geometric parameters to explore how internal stresses induced by the glass coating influence their magnetic properties and microstructure in different X_2YZ -based full-Heusler microwire series.

To prepare the Co_2FeSi alloys, arc melting was employed. The precursor elements—Co (99.99%), Fe (99.9%), and Si (99.99%)—were weighed according to the nominal composition ratio $(X)_2:(Y)_1:(Z)_1$ and placed in a graphite crucible (see Figure 2). The elements were melted together to form ingots of the respective alloys. To ensure homogeneity, the melting process was repeated five times. Before proceeding with glass coating, the chemical compositions and nominal ratios of the X_2YZ alloys were verified.

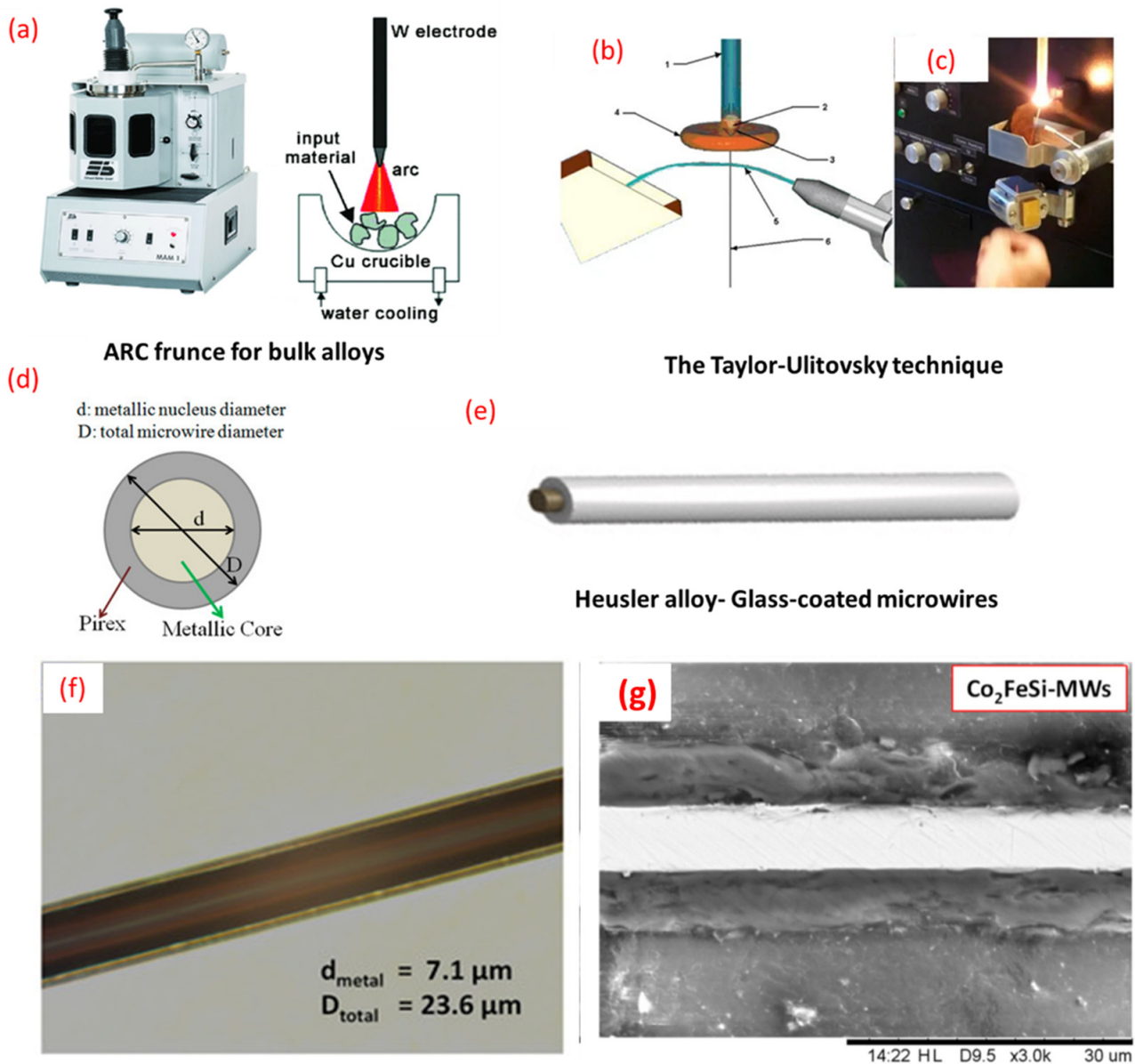


Figure 2. Image of the experimental steps facility for fabrication of thin Heusler based-glass-coated microwires: (a) arc melting furnace, (b,c) Taylor–Ulitovski method for production of glass-coated microwires, (d,e) Heusler-based glass-coated microwires sketch, (f) optical microscope, and (g) SEM images of Heusler-type Co_2FeSi glass-coated microwires.

Using the Taylor–Ulitsky technique, we produced a variety of Heusler-based glass-coated microwires with precisely controlled dimensions and lengths, tailored to specific applications and research objectives [86,88,93,100–105,108]. By regulating the casting rate during the melting process, we successfully obtained microwires with a consistent metallic nucleus diameter and a uniform glass coating thickness, ensuring fixed geometric parameters.

After fabricating the Co_2FeSi microwires (MWs), we determined their geometrical parameters—including metal core diameter (d_{metal}), total diameter (D_{total}), and aspect ratio ($\rho = d_{\text{metal}}/D_{\text{total}}$)—using optical microscopy, scanning electron microscopy (SEM), and energy-dispersive X-ray spectroscopy (EDX) (JEOL-6610LV, JEOL Ltd., Tokyo, Japan). The nominal chemical compositions of the samples were also analyzed. Once the chemical composition and nominal ratio were confirmed, microstructural characterization was performed at room temperature using X-ray diffraction (XRD) (D8 Advance, Bruker AXS GmbH, Karlsruhe, Germany).

Magnetic characterization was conducted in several steps. First, hysteresis (M-H) loops were measured at room temperature under magnetic fields applied parallel and perpendicular to the metallic core axis to evaluate magnetic anisotropy and confirm the easy axis of magnetization. Next, the magnetic behavior of the samples was examined over a broad temperature range (5–400 K) by recording M-H loops along the wire’s axis, representing the easy magnetization direction. Finally, thermal magnetization curves—specifically, field cooling (FC) and field heating (FH) curves—were analyzed under a low external magnetic field to investigate potential irreversibility or magnetic phase transitions in the Co_2FeSi MWs. All magnetization measurements were conducted using a PPMS (Physical Property Measurement System, Quantum Design Inc., San Diego, CA, USA) vibrating-sample magnetometer.

3. Results

3.1. Effect of Annealing Conditions

In this section, we highlighted the effect of the thermal treatment conditions on the magnetic and structure properties of Heusler-based glass-coated microwires.

3.1.1. Effect of Time Annealing in Co_2FeSi Glass-Coated Microwires

(a) XRD analysis

Figure 3 presents the morphological, compositional, and structural characterization of as-prepared and annealed Co_2FeSi glass-coated microwires, analyzed using scanning electron microscopy (SEM), energy-dispersive X-ray spectroscopy (EDX), and X-ray diffraction (XRD). The microwires exhibit a uniform cylindrical cross-section with a homogeneous elemental distribution (Figure 3a). EDX analysis (Figure 3b) confirms that the metallic nucleus composition, measured across 10 points (B1–B10), closely matches the nominal $\text{Co}_{50}\text{Fe}_{25}\text{Si}_{25}$ composition despite minor deviations from the stoichiometric Co_2FeSi . Annealed samples also maintain this composition, with a consistent Co:Fe atomic ratio of 2:1 and an average composition of $\text{Co}_{45}\text{Fe}_{22}\text{Si}_{33}$, aligning with previous findings on similar Co_2FeSi microwires [66]. The elevated Si content detected is attributed to an interfacial layer between the metallic core and glass coating, a characteristic feature of the fabrication process, as previously reported [66,75,78,103]. This interfacial layer, typically $\sim 0.5 \mu\text{m}$ thick, contributes significantly to the overall Si content, given the microwire diameter of approximately $4.36 \mu\text{m}$.

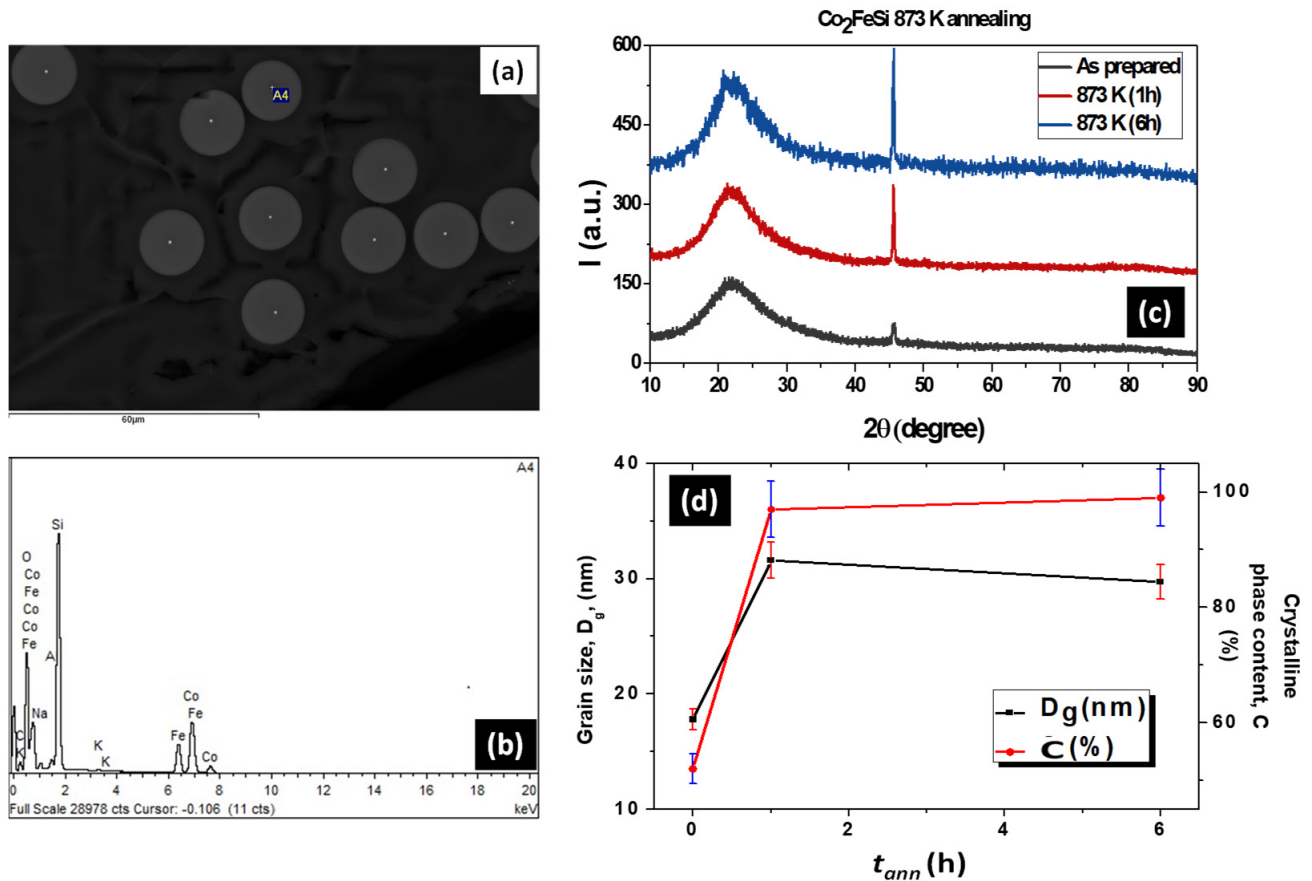


Figure 3. (a) SEM image showing the cross-section of as-prepared Co_2FeSi glass-coated microwires. (b) EDX spectrum from a selected point, confirming the presence of Co, Fe, and Si in the alloy. (c) X-ray diffraction (XRD) profile of as-prepared and annealed samples. (d) Variation in grain size (D_g) and crystalline phase content (C) with annealing time (t_{ann}) for Co_2FeSi glass-coated microwires.

XRD analysis (Figure 3c) reveals a broad peak centered at $2\theta \approx 22.5^\circ$, attributed to the amorphous glass coating [126,127]. Additionally, all samples exhibit a narrower peak at $2\theta \approx 46^\circ$, corresponding to a high-order $L2_1$ cubic metallic phase (space group: $Fm-3m$). Notably, the intensity of this peak increases significantly in annealed samples compared to the as-prepared ones, indicating recrystallization—a process consistent with the devitrification of amorphous microwires [103]. The measured lattice parameter of 5.640 Å aligns with values reported for similar compositions [75,78], further confirming the structural integrity of the material.

Figure 3d presents the calculated nanocrystalline grain size (D_g) using the Debye-Scherrer formula [103]:

$$D_g = K \lambda / \beta \cos 2\theta \quad (1)$$

where K is a shape factor (~ 0.94), λ is the XRD wavelength ($CuK\alpha$, $\lambda = 1.54 \text{ \AA}$), and β is the full width at half maximum (FWHM) of the peak at $2\theta \approx 46^\circ$ (Figure 1c).

The crystalline phase content (C) is determined from the total diffraction peak area, which includes both crystalline and amorphous contributions, using the following equation [48]:

$$C = \frac{I_c}{I_c + I_a (0.1 + e^{-D_g/25})} \quad (2)$$

where I_c and I_a are the integrated intensities of the crystalline and amorphous peaks, respectively, and 25 nm is a fitting constant [128].

Figure 3d shows a significant increase in D_g and C , from 17.8 nm and 52% (as prepared) to 31.6 nm and 97% (annealed at 873 K for 1 h). However, after 6 h of annealing, D_g slightly decreases to 29.7 nm, while C increases to 99%. The D_g values obtained for annealed Co_2FeSi are approximately four times higher than those reported for Co_2 -based Heusler alloy thin films [74,129]. This increase in D_g after annealing is commonly observed in most of materials due to a decrease in the energy of grain boundary through the grain boundary strengthening, the boundary migration, or changes in the dislocation density [129,130]. In particular, enhanced atomic diffusion at elevated temperatures can promote grain growth [95,131–134]. Additionally, the transformation of the amorphous phase into a bcc structure further contributes to grain growth with prolonged annealing.

As commonly observed, grain size increases during the devitrification of amorphous materials [132–134]. Crystallization involves grain nucleation and subsequent growth, which can be controlled either by atomic transfer at grain boundaries or by diffusion-driven nucleation mechanisms [133,134]. In nanocrystalline materials obtained via rapid quenching, the crystallization process is often more complex, sometimes leading to grain refinement [135]. A similar effect occurs here, where D_g decreases from 31.6 nm to 29.7 nm, possibly due to the nucleation of new nanograins or the dissolution of metastable grains followed by the formation of new nanocrystals [135]. This variation in grain size plays a crucial role in influencing the magnetization behavior of the samples, which will be discussed further.

(b) Magnetic properties

(i) Magnetic properties of as-prepared sample

Figure 4 presents the magnetic properties of as-prepared Co_2FeSi glass-coated microwires, showing the dependence of the magnetic moment (M) on the applied magnetic field (H) across a temperature range of 5–400 K with fields up to ± 50 kOe. As seen in Figure 4a,b, all M-H loops exhibit ferromagnetic behavior throughout the entire temperature range. The highest values of magnetic moment and remanence (M_r) are observed at 5 K, while the lowest values appear at 400 K. The hysteresis loops display a rectangular M-H shape, consistent with Co_2FeSi alloys produced by various deposition techniques and in different forms [56,136–138]. In the 200–400 K range, the loops show reduced saturation field (H_s), anisotropy field (H_k), remanence (M_r), and coercivity (H_c), as illustrated in Figure 4c,d.

The structure of the Co_2FeSi glass-coated microwires consists of a mixture of amorphous and crystalline phases. Due to this mixed structure, accurate determination of the anisotropy constant is challenging. In this study, the magnetic anisotropy field (H_k) was estimated from the hysteresis loops in Figure 4a,b and presented alongside with the coercivity (H_c) in Figure 4c. Notably, the nearly rectangular hysteresis loops observed here have also been reported in fully amorphous microwires and thin films [115,139,140], as well as in mixed amorphous–crystalline and nanocrystalline microwires [135]. Such rectangular shape of microwires has been attributed to shape magnetic anisotropy and the axial stresses induced by the difference in thermal expansion coefficients between the metallic nucleus and the glass coating.

Analysis of the M-H curves for Co_2FeSi glass-coated microwires (G-CMMWs) reveals a soft magnetic behavior, with the lowest coercivity ($H_c = 9$ Oe) detected at 200 K and the highest ($H_c = 25$ Oe) at 5 K, resulting in a variation of approximately 16 Oe. Similarly, the anisotropy field (H_k) exhibits its lowest value at 200 K and its highest at 5 K.

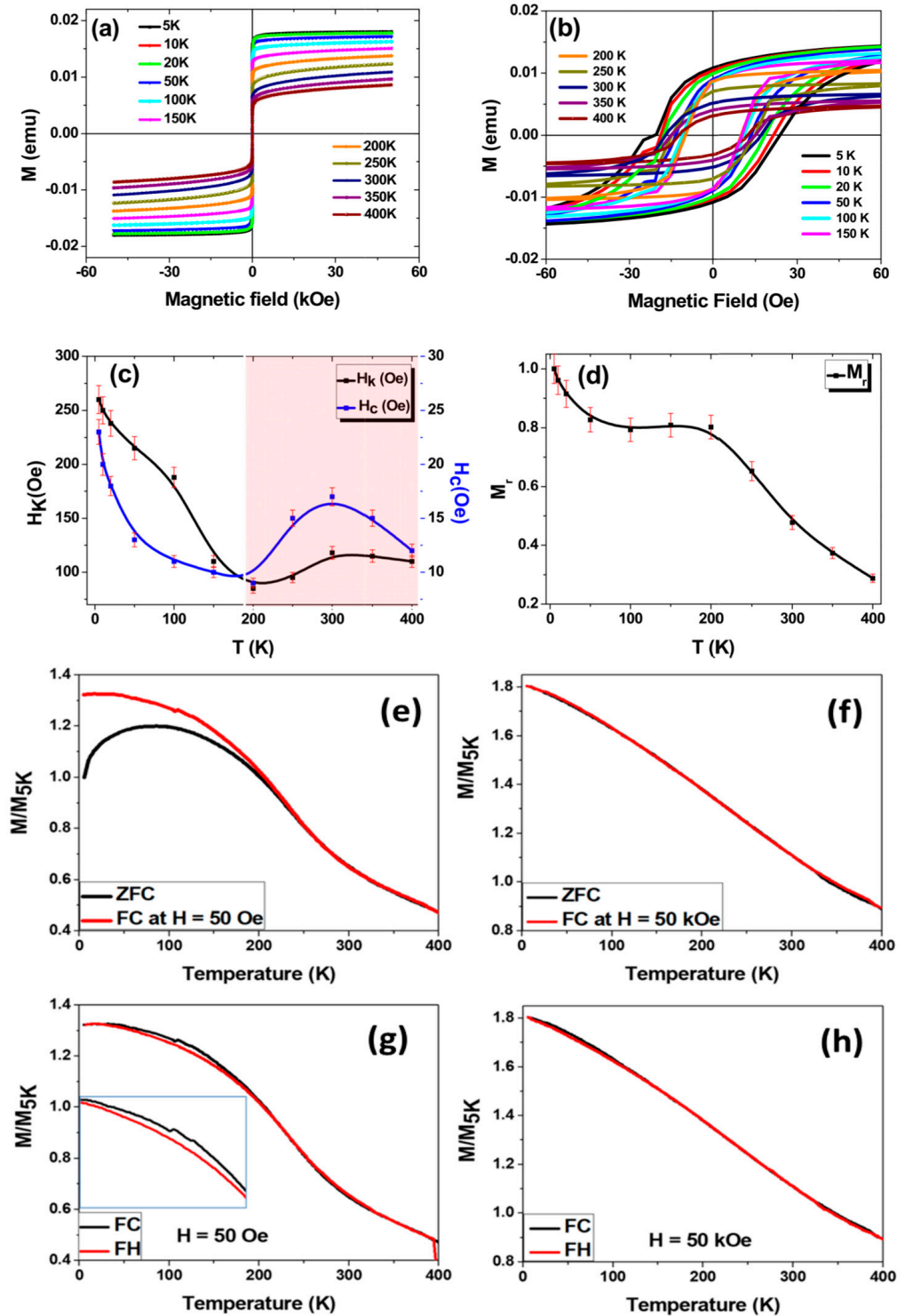


Figure 4. (a) Hysteresis loops of as-prepared Co_2FeSi glass-coated microwires, measured with a magnetic field applied parallel to the wire axis in the temperature range of 5–400 K, with field values between ± 50 kOe. (b) Hysteresis loops at a lower magnetic field scale. (c) Temperature dependence of coercivity and anisotropy field. (d) Normalized remanence as a function of temperature (lines serve as a visual guide). (e,f) Zero field cooling (ZFC) and field cooling (FC) of Co_2FeSi microwires at temperature range from 400 K to 5 K with different applied magnetic field (low magnetic field, 50 Oe and high magnetic field, 50 kOe, respectively). (g,h) FC from 400 K to 5 K and field heating (FH) from 5 K to 400 K of Co_2FeSi microwires with different applied magnetic field (low magnetic field, 50 Oe and high magnetic field, 50 kOe, respectively).

An unusual trend in H_c and H_k is observed (Figure 4c), where both parameters first increase as the temperature decreases from 400 K to 300 K, then decrease between 300 K and 200 K, and, finally, increase again, reaching their maximum at 5 K. This anomalous magnetic behavior has not been previously reported for Co_2FeSi alloys in other forms. It can be attributed to the internal stresses induced by the glass coating, which is temperature dependent and can affect the phase changes. These stresses, primarily caused by the thermal expansion mismatch between the metallic nucleus and the glass layer, can modify both the micromagnetic and crystalline structures, significantly affecting H_c and H_k [141].

The normalized remanence (M_r), defined as $M_r = M_r/M_{5k}$ (where is M_r at 5K), follows a more regular temperature-dependent trend (Figure 4d). It increases sharply from 0.28 to 0.81 as the temperature decreases from 400 K to 200 K, then stabilizes between 200 K and 100 K before rising again to reach its maximum at 5 K.

The temperature dependencies of M_r and H_c confirm the strong sensitivity of the magnetic properties of Co_2FeSi microwires to thermal variations. The anomalous behavior of H_c and H_k , alongside the expected trend of M_r , highlights the potential of these microwires for further studies on the effects of annealing and geometric factors. These findings could pave the way for utilizing Co_2FeSi microwires in spintronic devices based on thermo-magnetic switching.

Understanding the thermal stability of ferromagnetic materials is crucial for their application in spintronic devices, particularly in determining their performance at, below, or above room temperature (RT). To assess this, the temperature dependence of magnetization (M vs. T) was measured under different conditions, zero-field cooling (ZFC), field cooling (FC), and field heating (FH), using both low ($H = 50$ Oe) and high ($H = 50$ kOe) magnetic fields over a temperature range of 4 to 400 K (Figure 4e–h). To facilitate comparison, the M vs. T curves were normalized to the maximum magnetic moment at 5 K.

In the FC protocol, the Co_2FeSi G-CMMWs were cooled to 4 K under an applied magnetic field, aligning the magnetic moments parallel to the field. In contrast, in the ZFC system, the moments remained randomly oriented. As the temperature increased under a low external field, the magnetic moments aligned with the applied field, leading to an increase in magnetization until relaxation effects became dominant, causing ZFC to decrease and eventually merge with FC at higher temperatures [142].

A significant magnetic irreversibility was observed at low fields ($H = 50$ Oe), with a blocking temperature (T_B) of ~205 K (Figure 4e). However, this irreversibility disappeared under a high magnetic field ($H = 50$ kOe) (Figure 4h), confirming that it is strongly dependent on the field strength. Such behavior, commonly reported in magnetic materials, results from the coexistence of re-entrant ferromagnetism and spin glass-like behavior [143,144].

Additionally, the disordered structure and chemical composition of Co_2FeSi G-CMMWs contribute to this phenomenon. The magnetic ground state is not purely ferromagnetic; instead, a random spin-disordered B2 phase coexists with the ferromagnetic $L2_1$ phase [142,143]. This mixed-phase structure is induced by internal stresses from the glass coating during fabrication, leading to the formation of both disordered (B2) and ordered ($L2_1$) phases, alongside the amorphous phase, as confirmed by XRD analysis. Notably, applying a high magnetic field (50 kOe) suppressed the B2 phase, eliminating the irreversibility behavior.

(ii) Magnetic properties of annealed samples

Figure 5 presents the hysteresis loops of as-prepared and annealed Co_2FeSi glass-coated microwires at different annealing temperatures (T_{ann}) measured at room temperature with the magnetic field applied parallel to the microwire axis. All samples exhibit ferromagnetic behavior, with the transition to the paramagnetic phase occurring above 1100 K [64]. The as-prepared sample (Figure 5a) shows soft magnetic behavior with a narrow, non-

squared loop. The relatively soft magnetic properties of the as-prepared sample can be linked to its nanocrystalline structure with D_g below 20 nm. In contrast, the annealed samples (Figure 5b,c) display harder magnetic behavior with more rectangular hysteresis loops. These shape of the hysteresis loops, with a reduced remanent magnetization ($M/M_{\max} \approx 0.97$) and higher H_c , suggest either the development of axial magnetic anisotropy, with the axial easy magnetization axis aligned with the direction of the applied field, or magnetic hardening due to increase in D_g . An increase in D_g up to 30–35 nm (see Figure 3d) and the induction of strong cubic magnetocrystalline anisotropy (CMA) along the (220) direction parallel to the microwire axis after annealing have been previously reported [139]. In contrast, the as-prepared sample predominantly exhibits uniaxial magnetic anisotropy (UMA), with a smaller contribution from CMA. The annealing conditions enhance the CMA, leading to modification in key magnetic parameters such as remanence (M_r), anisotropy field (H_k), and coercivity (H_c), as shown in Figure 5d.

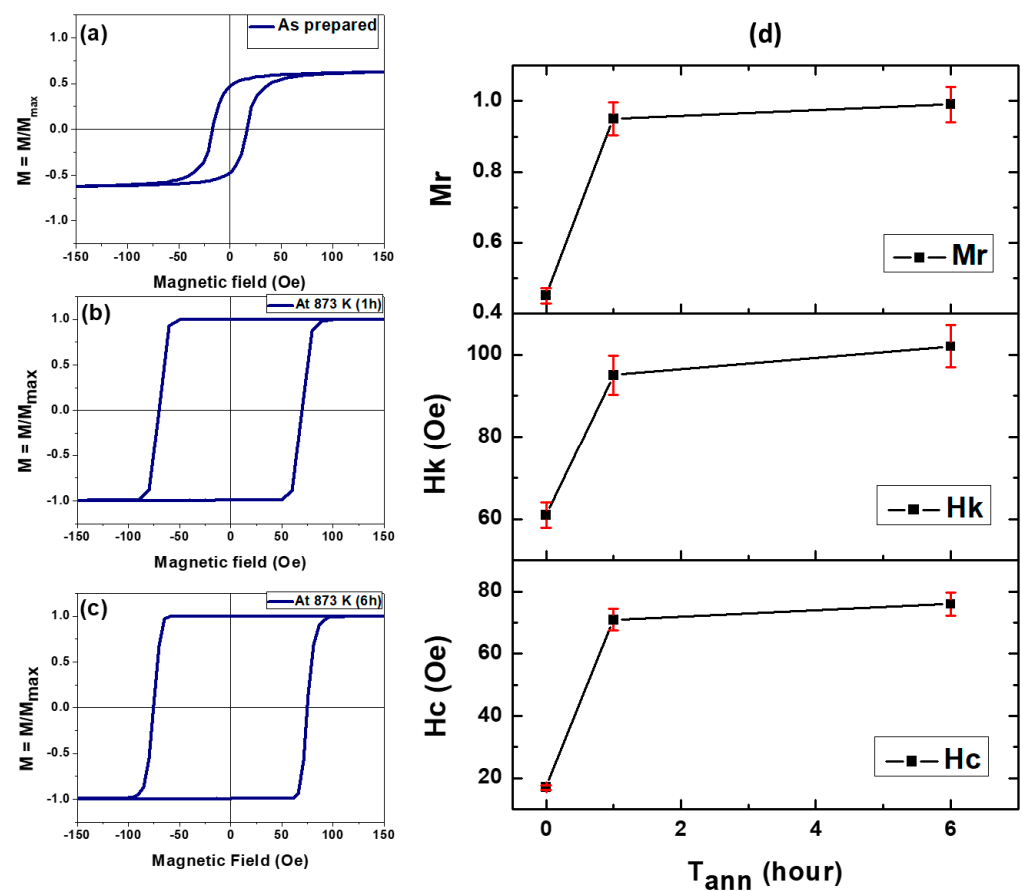


Figure 5. Hysteresis loops of Co_2FeSi G-CMMWs: (a) as prepared, (b) annealed at 873 K for 1 h, and (c) annealed at 873 K for 6 h. All loops were measured at room temperature. (d) The dependence of coercivity, anisotropy field, and remanence on annealing time for Co_2FeSi G-CMMWs is shown (lines are for eye guide).

The thermal stability of ferromagnetic materials is crucial for their potential use in spintronic devices. Notably, we observed a significant increase in coercivity (H_c), remanence (M_r), and anisotropy field (H_k) after annealing (Figure 6), confirming that cubic magnetocrystalline anisotropy (CMA) dominates in the annealed samples up to 400 K. Analyzing the M-H curves at different temperatures (5–400 K) for both as-prepared and annealed Co_2FeSi microwires, we observed an interesting temperature dependence of H_c and M/M_{\max} -values, with respect to the highest magnetic moment at 5 K (see Figure 6a). The unusual behavior of the H_c of the as-prepared sample between 400 K and 200 K could

be attributed to the competition between uniaxial magnetic anisotropy (UMA) and cubic magnetocrystalline anisotropy (CMA).

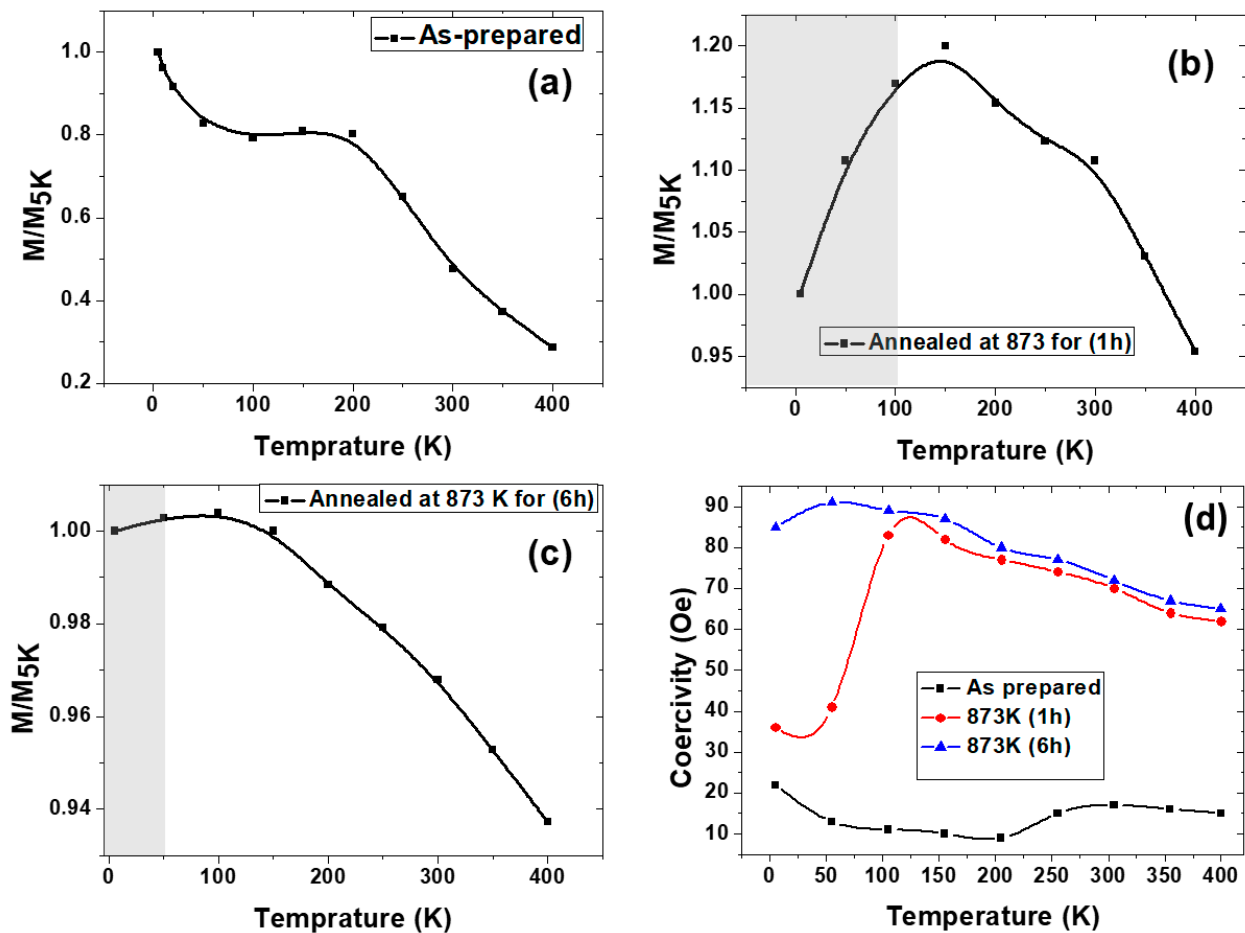


Figure 6. Temperature dependence of the remanence for samples (a) as prepared, (b) annealed at 873 (1 h), and (c) annealed at 873 K for 6 h. (d) Coercivity of Co_2FeSi microwire investigated samples. Lines for eye guide.

For the annealed samples, H_c and M_r are higher across the full temperature range compared to the as-prepared sample. Notably, H_c and M_r exhibit matching trends, indicating uniform magnetic anisotropy for all temperatures, unlike in the as-prepared sample (Figure 6). For the annealed sample at 1 h, H_c and M_r show a maximum at 150 K, followed by a flipping temperature point (T_f), where both parameters decrease as temperature decreases, reaching their lowest values at 5 K. A similar behavior is observed for the 6 h annealed sample but with the flipping point occurring at 55 K (Figure 6b–d). Moreover, we noticed a change in the M-H loops for the annealed samples at 1 h and 6 h below T_f . Above T_f , the hysteresis loops exhibit a single-step magnetic reversal with square loops. Below T_f , the loops show a multi-step magnetization reversal process, with a distorted shape, as indicated in Figure 7. This behavior has been observed in various magnetic materials, including magnetic nanostructured thin films, nanoparticles, and magnetic microwires with mixed amorphous–crystalline structure [145–147]. To our best knowledge, this is the first time that such magnetic behavior has been observed in annealed Co_2FeSi alloy glass-coated microwires. This suggests that there is a critical temperature at which this unusual behavior arises, likely related to the nanocrystalline structure and grain size. We can deduce that even small changes in the grain size (D_g) can significantly affect the magnetic behavior.

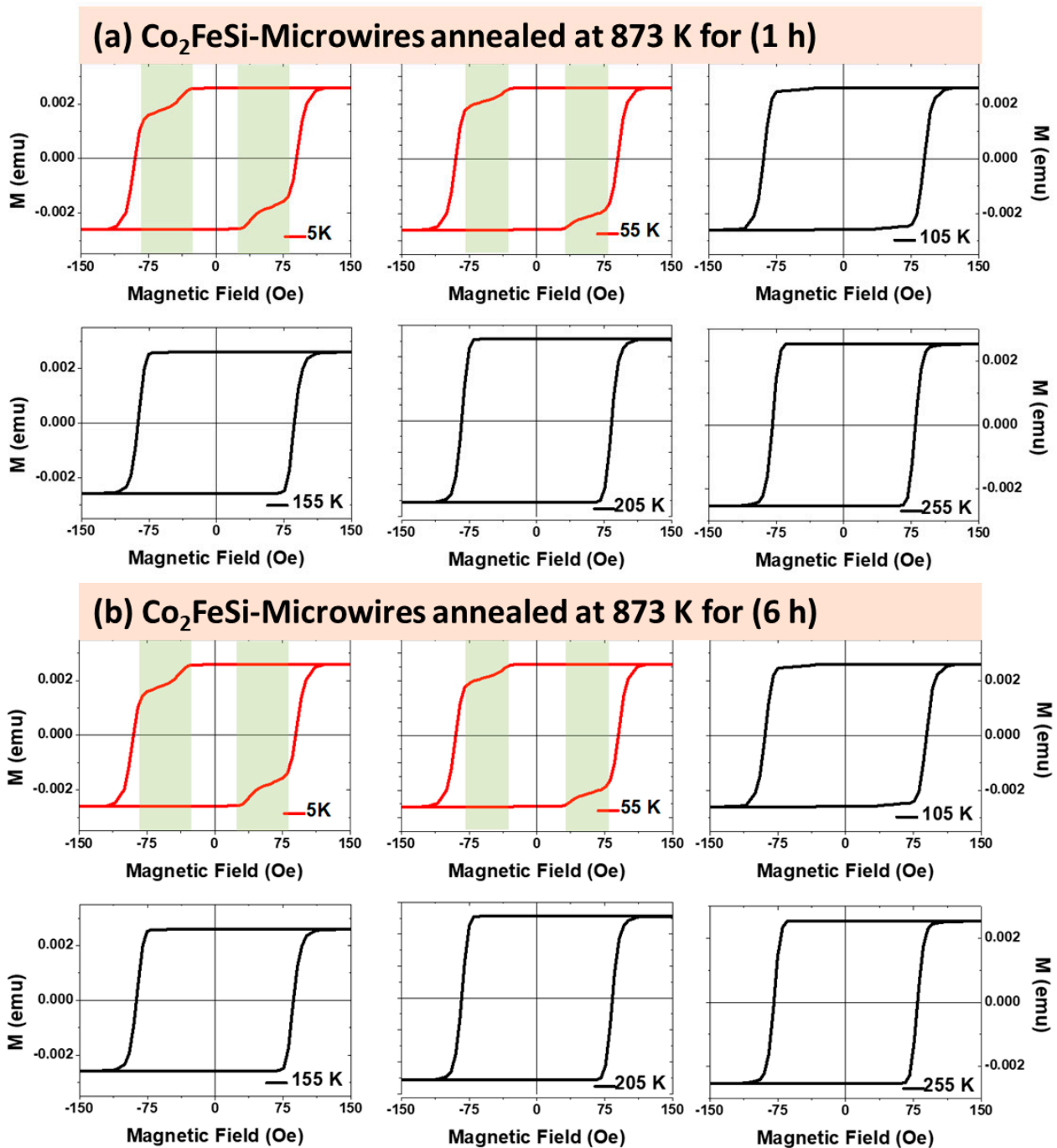


Figure 7. Hysteresis loops measured in a magnetic field applied parallel to the axis of the microwires over the temperature range from 5 to 255 K for annealed Co_2FeSi microwires at 873 K for 1 h (a) and 6 h (b).

Multi-Step Magnetic Behavior and the Role of Nanocrystallinity in Co_2FeSi Microwires

An unusual multi-step magnetic behavior emerges in glass-coated Co_2FeSi microwires, strongly influenced by the superposition effect of an external magnetic field and the microwire's stray field. This phenomenon, reported in previous studies [22,25,35,145,148,149], can be attributed to the mixed structure of studied samples [145], fluctuations in the metallic nucleus diameter, or the magnetostatic interaction of the magnetic microwires [150]. The strength of this superposition effect depends on the difference between the stray and switching fields, intensifying when this difference increases. A remarkable finding is that at low temperatures, a single microwire behaves as if composed of two distinct magnetic

microwires due to the pronounced difference between the two fields. This results in the multi-step magnetization process, which is absent in as-prepared samples due to their small nanocrystalline grain size (D_g). This observation strongly suggests that annealing significantly affects the nanocrystalline structure (D_g -value), leading to the formation of two magnetic phases with distinct behaviors, ultimately triggering the multi-step magnetic response. Below the critical temperature (T_f), the switching fields of these magnetic phases diverge. Once one phase undergoes magnetization switching, the combined effect of the external field and the demagnetizing field from the already re-magnetized phase is insufficient to switch the second phase, which possesses a larger moment. This effect is further amplified by the presence of 50% Co (soft phase) and 25% Fe (hard phase) in the annealed samples, which contributes to hysteresis loop distortions and the multi-step magnetization reversal process.

Magnetic Phase Transitions and Thermal Effects

To explore the thermo-magnetic behavior and potential magnetic phase transitions, field-cooling (FC) and field-heating (FH) curves were measured under low magnetic fields. As-prepared samples (Figure 8a) exhibit a stable ferromagnetic state between 400 K and 190 K, with FC and FH curves coinciding. However, below 190 K, a small gap emerges between them, with FC rising above FH before they realign at 15 K. This suggests a magnetic phase transition, consistent with previous findings [66,75,78,151–153]. Notably, changes in H_c and M_r below 200 K (Figure 6) indicate a strong correlation between these parameters and the observed magnetic phase transition. Annealed samples at 873 K (Figure 8b,c) display more complex behavior. For the 1 h annealed sample, a sharp drop in magnetization occurs under a 50 Oe external field, suggesting a pronounced magnetic phase transition (Figure 8b). In contrast, for the 6 h annealed sample, this drop disappears, and a separation between FC and FH emerges only below 105 K, with the curves matching again at 60 K—another indication of a magnetic phase transition (Figure 8c). The blocking temperature (T_b) for the 1 h sample is 150 K, aligning precisely with the critical flipping temperature (T_f), reinforcing the idea that the nanocrystalline structure significantly influences magnetic transitions. These results demonstrate that Co_2FeSi Heusler alloys are highly sensitive to annealing conditions, which directly affect their lattice structure, local atomic arrangement, and stoichiometric composition [74]. The annealing at 873 K for 1 h and 6 h promotes recrystallization, accompanied by atomic ordering, the reduction of internal stresses, and the formation of two distinct magnetic phases with different magnetic responses, leading to the observed anomalous magnetic behavior in annealed Co_2FeSi microwires.

3.1.2. Effect of Annealing Temperature in Co_2FeSi Glass-Coated Microwires

Figure 9a–f presents the M-H loops of annealed Co_2FeSi microwires measured at varying temperatures, from 305 K to 5 K. Regardless of temperature, all samples exhibit ferromagnetic behavior, both above and below room temperature. Above room temperature, the hysteresis loops maintain a rectangular shape, with a gradual reduction in coercivity (H_c), saturation magnetization (M_s), and remanent magnetization (M_r) as the temperature increases, following the same trend as the as-prepared Co_2FeSi samples. However, for Co_2FeSi microwires annealed at 873 K and 973 K, a drastic shift in magnetic behavior emerges below room temperature. At critical temperatures of 105 K and 255 K, respectively, significant distortions appear in the hysteresis loops, evolving into a distinctive “kink” or “wasp-waisted” magnetic behavior, characterized by multi-step magnetic switching. Above these critical temperatures, the loops maintain a regular shape, but below them, the multi-step hysteresis loops are observed.

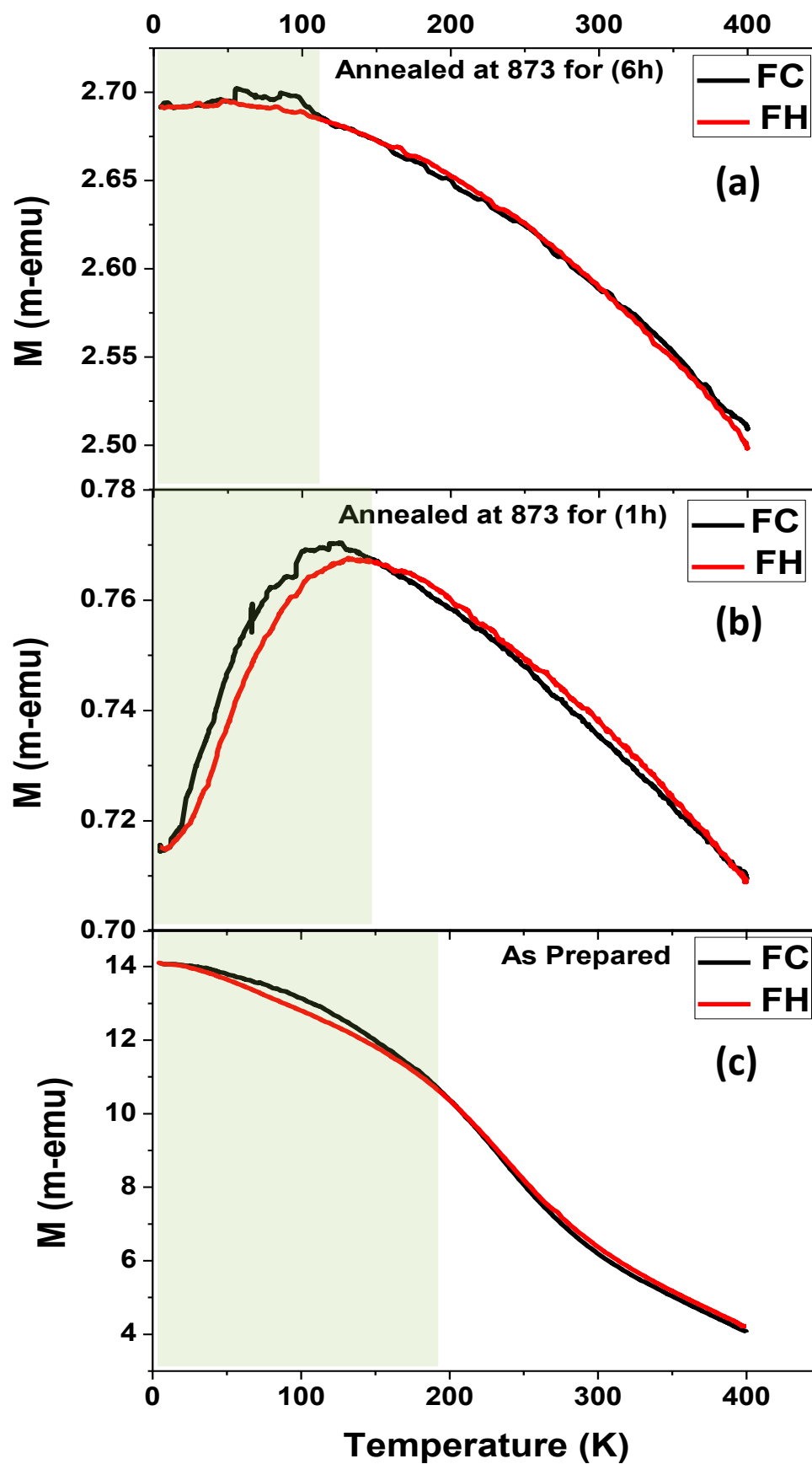


Figure 8. Temperature dependence of magnetization measured for Co_2FeSi glass-coated microwires (a) annealed at 873K for 6 h, (b) annealed at 873 K for 1 h, and (c) as prepared with applied external magnetic field 50 Oe.

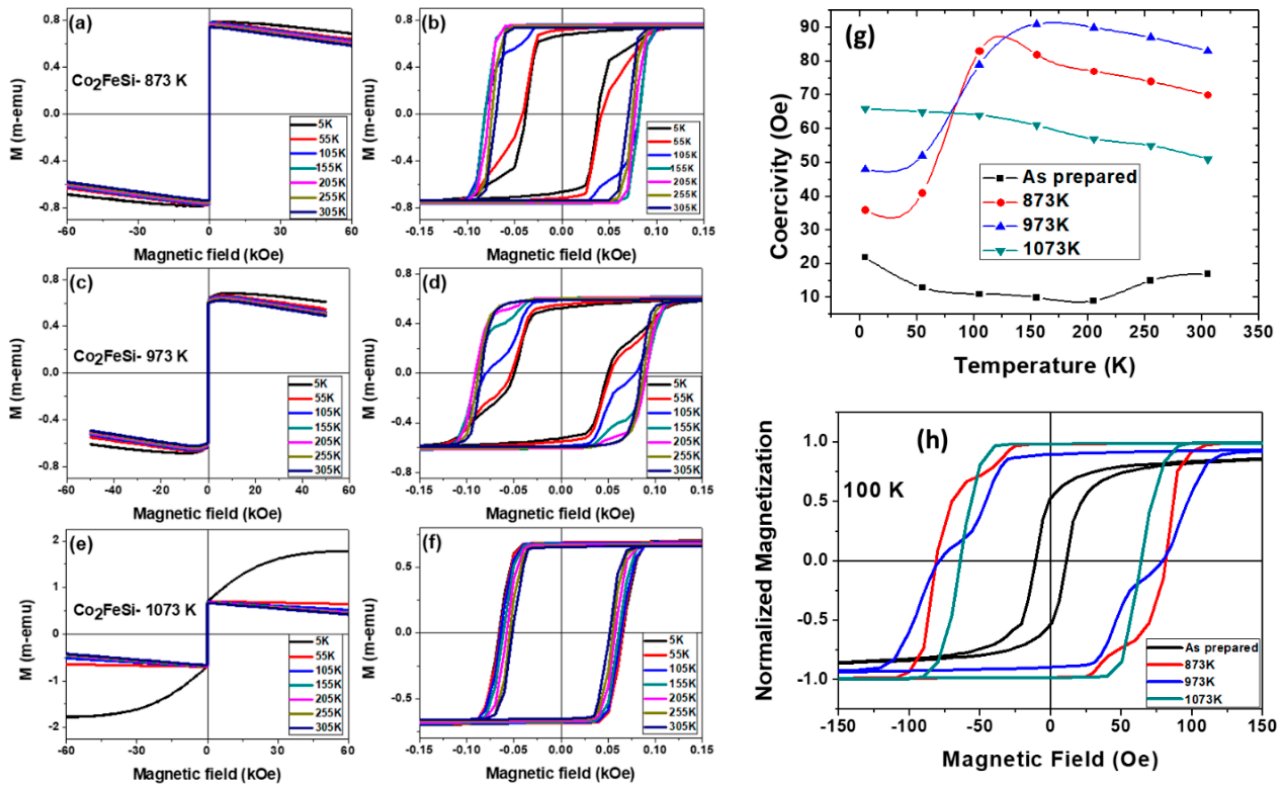


Figure 9. Hysteresis loops of Co_2FeSi microwires annealed at different temperatures for 1 h, measured with the magnetic field applied parallel to the microwire axis over a temperature range of 5 to 305 K: (a,b) 873 K, (c,d) 973 K, and (e,f) 1073 K. (g) Temperature-dependent coercivity (H_c) for as-prepared and annealed samples at various temperatures (lines serve as a visual guide). (h) Hysteresis loops recorded at 100 K for as-prepared and annealed Co_2FeSi microwires at 873 K, 973 K, and 1073 K, with the magnetic field applied along the microwire axis.

Interestingly, this type of magnetic response is well-documented in magnetic nanoparticles, nanostructured thin films, and amorphous microwires, yet it is first observed in Co_2FeSi alloy glass-covered microwires. Several mechanisms have been proposed to explain such behavior:

- Strong magnetic coupling between distinct magnetic phases (in this case, hard Co and soft Fe regions), leading to an oxidation-induced imbalance.
- Reordering of ferromagnetic spins below the critical temperature under an applied magnetic field, causing domain wall pinning and influencing hysteresis loop distortions.
- Superposition of an external magnetic field and the stray field from the microwire array, induced by factors such as metallic nucleus diameter fluctuations or mixed crystalline structure.

A particularly fascinating aspect of this study is that multi-step behavior is absent in as-prepared samples—it only emerges in samples annealed at 873 K and 973 K, disappearing again at 1073 K. This suggests that annealing induces two distinct magnetic phases with different responses, tightly linked to the critical temperature where multi-step switching occurs. Below this temperature, the coercive field of each magnetic phase varies. When one phase switches, the combined effect of its demagnetizing field and the external magnetic field is insufficient to trigger magnetization switching in the second phase, leading to the multi-step process. Moreover, the presence of 50% Co (responsible for magnetically hard phase) and 25% Fe (magnetically soft phase) in annealed samples can play a relevant role in shaping the “kink” or “wasp-waisted” hysteresis loops and reinforcing the multi-step magnetic behavior.

An unusual coercive field trend with temperature has been observed while analyzing the magnetic hysteresis loops of as-prepared and annealed Co_2FeSi samples (Figure 9g). All annealed samples exhibit a higher H_c compared to the as-prepared one. For the as-prepared sample, a soft magnetic behavior is evident, with only a slight variation in H_c between 305 K (18 Oe) and 5 K (21 Oe), indicating a minimal change of just 3 Oe over the temperature range. However, for samples annealed at 873 K and 973 K, an anomalous coercivity trend emerges. Initially, H_c increases as the temperature decreases, reaching a maximum at 105 K and 155 K, respectively. Below these critical points, H_c unexpectedly decreases with further cooling, reaching its lowest value at 5 K. Interestingly, this anomalous coercivity behavior disappears in samples annealed at 1073 K, suggesting a direct link between annealing conditions and the magnetic phase transitions. This peculiar coercivity trend aligns perfectly with the critical temperature of the multi-step magnetic switching observed in Figure 9h. Specifically, above the critical temperature, the samples exhibit regular ferromagnetic behavior with a single-step switching mechanism. Below the critical temperature, the hysteresis loops transform, displaying the characteristic multi-step magnetization reversal. In typical crystalline and polycrystalline ferromagnetic materials, decreasing the temperature generally enhances magnetic anisotropy, leading to a natural increase in H_c . However, in this case, the shift in coercivity at low temperatures is strongly tied to micromagnetic structure changes, driven by transformations in the magnetic phases (as discussed in Figure 9a–f).

Figure 10 displays the temperature dependence of magnetization for Co_2FeSi microwires. As shown in Figure 10a, the as-prepared sample exhibits strong ferromagnetic behavior across the entire temperature range: The magnetization changes from its maximum values at 5 K to its minimum at 400 K, which is typical for ferromagnetic materials. This M vs. T behavior explains the regular magnetic behavior observed in the H_c and M - H loops at different temperatures for the as-prepared Co_2FeSi sample. Additionally, the Curie temperature (T_c) of the as-prepared sample could not be directly measured from the M vs. T curve, as it is expected to be above 1100 K, which is beyond the maximum temperature (400 K) of the employed PPMS device. For the annealed samples at 873 K and 973 K, a magnetic phase transition is observed, as indicated by a sharp drop in magnetization when external magnetic fields of 50 Oe and 200 Oe are applied during field-cooled (FC) and field-heated (FH) measurements, as shown in Figure 10b,c. Notably, this sharp drop disappears when a higher field of 1 kOe is applied to both annealed samples. These magnetic phases, observed in the annealed samples, are linked to the anomalous magnetic behavior described in Figure 9. The blocking temperatures (TB) for the samples annealed at 873 K and 973 K are found to be 150 K and 205 K, respectively, which aligns with the critical temperature suggested earlier for these samples. The as-prepared sample and the sample annealed at 1073 K do not show any irreversible behavior (Figure 10a,d). Thus, Co_2FeSi Heusler alloys are sensitive to annealing conditions, which affect both the lattice structure and the local atomic environment, as well as their stoichiometric composition. The anomalies observed in the M vs T curves for magnetic Heusler alloys are often explained by three main phase transition temperatures: the Curie temperature of the martensitic (TCM) phase, the martensitic transition temperature (TM), and the Curie temperature of the austenitic cubic phase at high temperatures. In this case, the martensitic transition temperature is more relevant since T_c for the annealed samples at 873 K and 973 K is expected to be much higher than TM. Moreover, the TM range coincides with the critical temperature where the “kink” or “wasp-waisted” hysteresis loops and multi-step magnetic behavior are observed. We suggest that the annealing at 873 K and 973 K induces recrystallization, atomic ordering, and the reduction of internal stresses, leading to the formation of two distinct magnetic

phases. The martensitic phase with a different magnetic response is responsible for the observed anomalous magnetic behavior in the annealed Co_2FeSi .

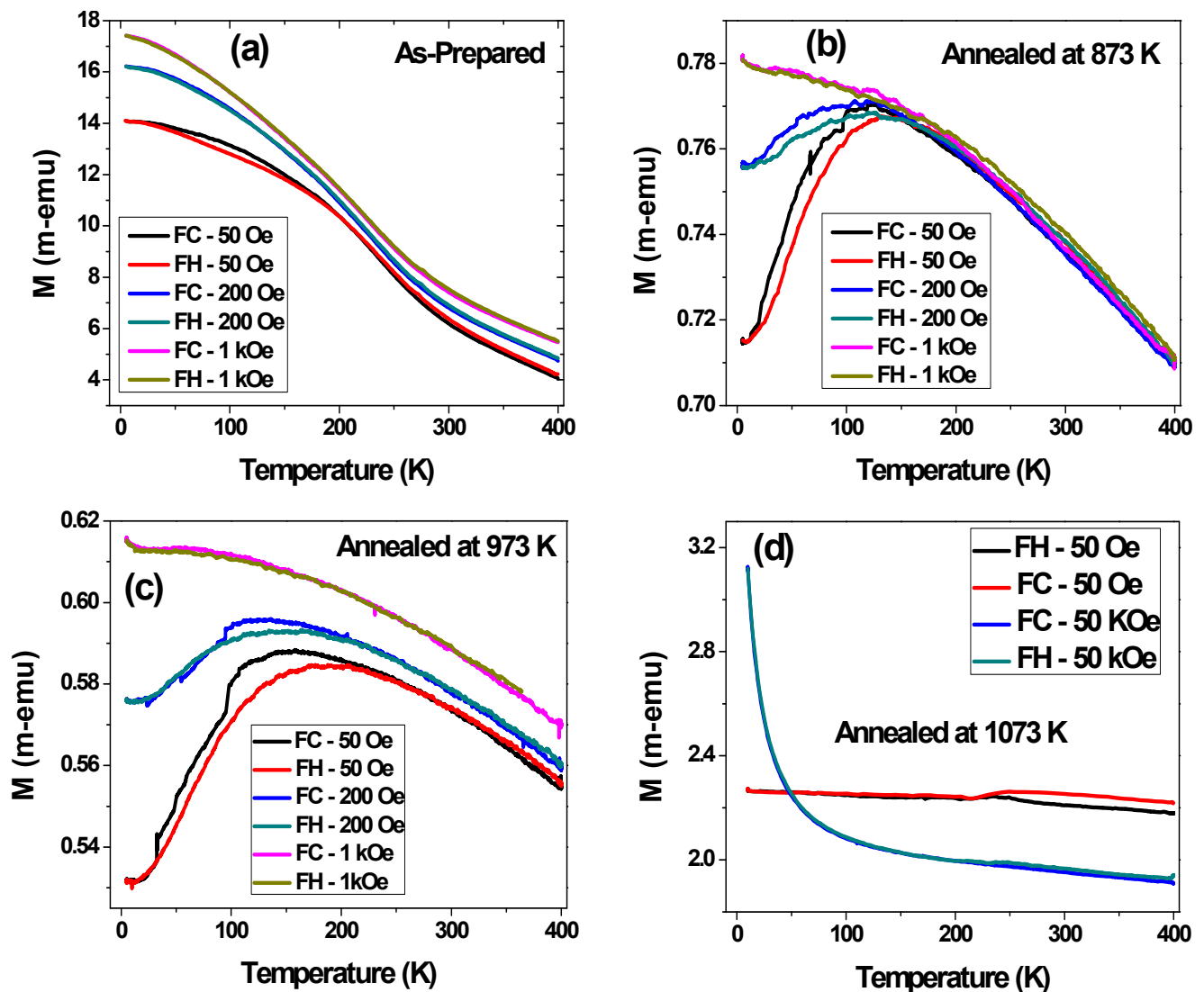


Figure 10. Temperature-dependent magnetization curves for Co_2FeSi microwires measured under different applied magnetic fields for samples (a) as-prepared, (b) annealed at 873 K, (c) annealed at 973 K, and (d) annealed at 1073 K.

4. Potential Applications

Heusler alloy glass-coated microwires, with their unique combination of properties including thermal stability, high Curie temperatures, tunable magnetic behavior, and enhanced mechanical and chemical resistance due to the glass coating, hold significant promise for a variety of advanced applications.

4.1. Spintronic Devices

The unique combination of high spin polarization, tunable magnetic properties, and thermal stability makes Heusler alloy glass-coated microwires promising candidates for various spintronic devices. Spintronics leverages the spin of electrons in addition to their charge, enabling the development of faster, more power-efficient, and non-volatile memory and logic devices. Co_2 -based Heusler alloys, in particular, are of great interest due to their predicted half-metallicity, where electrons of one spin orientation are metallic while others are insulating, leading to nearly 100% spin polarization at the Fermi level. Achieving and

maintaining this high spin polarization, particularly in the ordered L2₁ phase, is crucial for spintronic applications [154–164].

Specifically, these microwires are attractive for the following applications:

- Spin valves and magnetic tunnel junctions (MTJs): Spin valves and MTJs are fundamental building blocks of spintronic devices. They consist of ferromagnetic layers separated by a non-magnetic metal (spin valve) or an insulating layer (MTJ). The resistance of these structures depends on the relative orientation of the magnetization in the ferromagnetic layers, a phenomenon known as giant magnetoresistance (GMR) or tunneling magnetoresistance (TMR). Heusler alloys, with their high spin polarization, are excellent candidates for the ferromagnetic electrodes in MTJs, leading to high TMR ratios, which are essential for device performance. The ability to control the magnetic properties of microwires through annealing and compositional variations allows for the fine-tuning required for optimal spin valve and MTJ performance.
- Magnetic random access memory (MRAM): MRAM is a non-volatile memory technology that stores data using magnetic states. Different MRAM technologies exist, including Spin-Transfer Torque MRAM (STT-MRAM) and Spin-Orbit Torque MRAM (SOT-MRAM). In STT-MRAM, the magnetization of a free layer is switched by a spin-polarized current. SOT-MRAM utilizes spin–orbit interactions in a heavy metal layer to generate a spin current that switches the magnetization. Heusler alloys with high spin polarization and low damping are highly desirable for the magnetic layers in both STT-MRAM and SOT-MRAM, offering potential for high-speed and low-power operation. The thermal stability and potential for miniaturization offered by Heusler alloy microwires are advantageous for the development of high-density MRAM [160–165].
- Domain wall devices: The controlled manipulation of magnetic domain walls in ferromagnetic nanostructures is another promising avenue for spintronic applications, including logic and memory devices. The observed magnetic behavior in Heusler alloy microwires, such as the multi-step magnetization reversal, suggests their potential for use in domain wall-based devices. The geometry and internal stress distribution in microwires can influence domain wall dynamics, offering possibilities for tailoring their behavior for specific functionalities [112].

4.2. Magnetic Sensors

The sensitivity of the magnetic properties of Heusler alloy microwires to external stimuli like magnetic fields and temperature makes them highly suitable for sensor applications. Their soft magnetic behavior, which can be tuned by controlling factors such as geometric parameters and annealing conditions, allows for the development of sensitive magnetic field sensors. The ability to tailor parameters like coercivity and anisotropy is crucial for optimizing sensor performance. Furthermore, the distinct temperature dependence of the magnetic properties, including the observed magnetic phase transitions, can be effectively exploited for temperature-sensing applications. Glass-coated magnetic microwires, in general, have shown promise in various sensing applications due to their specific magnetic domain structure and high magnetoimpedance effect, offering advantages in terms of sensitivity and miniaturization compared to some other materials [101,115,117,166–169].

4.3. Biomedical Engineering

Heusler alloy glass-coated microwires hold significant potential in biomedical engineering, owing to their unique magnetic properties and the inherent biocompatibility provided by the glass coating. One key application is in magnetic hyperthermia, where the ability of these materials to generate heat upon exposure to an alternating magnetic field can be utilized for targeted cancer therapy. The localized heating can selectively

destroy cancer cells with minimal damage to surrounding healthy tissue. Additionally, the sensitivity of the magnetic properties to biological molecules suggests their potential for developing novel biosensors. While specific *in vivo* or *in vitro* studies on Co₂FeSi microwires are subjects for future research, the broader class of glass-coated magnetic microwires has been explored for biomedical applications, including magnetic hyperthermia for *in vitro* cancer cell treatment [101,115,117,118,170].

4.4. Other Potential Applications

Beyond spintronics and sensing, Heusler alloy glass-coated microwires present exciting possibilities for other advanced applications. The magnetocaloric effect, where a temperature change is induced by a changing magnetic field, is observed in some Heusler alloys and suggests their potential for energy-harvesting devices. This effect could be utilized in solid-state cooling or for converting waste heat into usable energy. Furthermore, the magnetic field-induced shape memory effects observed in certain Heusler alloys could be harnessed for the development of microactuators. These micro-scale devices could find applications in various fields, including minimally invasive surgery or microfluidics. The tunable properties of Heusler alloy microwires make them versatile materials for exploring these and other novel functionalities.

5. Challenges and Future Works

While significant progress has been made in the fabrication and characterization of Heusler alloy glass-coated microwires, several challenges remain, and future research directions can be identified.

5.1. Precise Control of Microstructure

- Achieving precise control over the microstructure, particularly the degree of L₂₁ ordering and the grain size distribution, remains a challenge.
- Future work should focus on optimizing fabrication parameters, such as annealing conditions and cooling rates, to enhance structural order and tailor the microstructure for specific applications.

5.2. Understanding Complex Magnetic Behavior

- The complex magnetic behavior observed in these microwires, including the multi-step magnetization reversal and the interplay between different magnetic anisotropies, requires further investigation.
- Future studies should aim to develop a deeper understanding of the underlying mechanisms governing these phenomena, potentially through advanced micromagnetic modeling and simulation.

5.3. Integration into Devices

- While the potential applications of Heusler alloy microwires are promising, their integration into actual spintronic devices, sensors, and biomedical technologies presents challenges.
- Future research should focus on developing reliable methods for device fabrication, addressing issues such as microwire alignment, electrical contacting, and compatibility with other device components.

5.4. Exploring New Materials and Compositions

- The current review primarily focuses on Co₂FeSi alloys. Future work should explore other Heusler alloy compositions and even quaternary or quinary alloys to discover new materials with enhanced properties.

- Investigating the effects of doping or introducing other elements into the microwires could also lead to novel functionalities.

5.5. *In Situ Characterization*

- In situ characterization techniques, such as real-time monitoring of microstructure evolution during annealing or magnetic measurements under applied stress, would provide valuable insights into the structure–property relationships in these materials.
- Developing and utilizing such techniques should be a priority for future research.

5.6. *Modeling and Simulation*

- Computational modeling and simulation can play a crucial role in complementing experimental studies.
- Future efforts should focus on developing accurate models to predict the structural, magnetic, and electronic properties of Heusler alloy microwires, aiding in the design of materials with tailored properties.

6. Conclusions

This review has provided a comprehensive overview of recent advancements in the fabrication, structural characterization, and magnetic properties of Co₂FeSi Heusler alloy glass-coated microwires. The Taylor–Ulitsky method has proven to be a versatile technique for producing microwires with controlled dimensions and enhanced properties. The ability to tune the magnetic properties of these microwires through variations in composition, annealing conditions, and geometric parameters opens up a wide range of potential applications, particularly in spintronics, magnetic sensing, and biomedical fields. However, challenges such as achieving precise control over the L₂₁ ordering, understanding complex magnetic phenomena like multi-step magnetization reversal, and integrating microwires into devices need to be addressed. Future research should focus on these areas, as well as exploring new Heusler alloy compositions and developing advanced characterization techniques, to fully realize the potential of these remarkable materials.

Author Contributions: Conceptualization, M.S., J.G. and A.Z.; methodology, M.S., J.M.B. and V.Z.; validation, M.S., V.Z., J.M.B. and A.Z.; formal analysis, M.S.; investigation, M.S., V.Z., J.G., J.M.B. and A.Z.; resources, J.G., V.Z. and A.Z.; data curation M.S. and V.Z.; writing—original draft preparation, M.S. and A.Z.; writing—review and editing, M.S. and A.Z.; visualization, M.S. and V.Z.; supervision, J.G. and A.Z.; project administration, J.G., V.Z. and A.Z.; funding acquisition, J.G., V.Z. and A.Z. All authors have read and agreed to the published version of the manuscript.

Funding: The research was made possible by funding from the Spanish MICIN (project PID2022-141373NB-I00), by EU (Horizon Europe) under “INFINITE” (HORIZON-CL5-2021-D5-01-06) and “HARMONY” (HORIZON-CL4-2023-RESILIENCE-01) projects, Basque Government Elkartek projects “ATLANTIS” and “MOSINCO”, and the “Ayuda a Grupos Consolidados” grant (IT1670-22). M.S. acknowledges the Maria Zambrano contract funding from the Spanish Ministerio de Universidades and EU—Next Generation EU.

Data Availability Statement: The original contributions presented in this study are included in the article. Further inquiries can be directed to the corresponding authors.

Acknowledgments: The authors thank the technical and human support provided by SGIker of UPV/EHU (Medidas Magneticas Gipuzkoa) and European funding (ERDF and ESF).

Conflicts of Interest: The authors declare no conflicts of interest.

References

1. Li, T.; Pickel, A.D.; Yao, Y.; Chen, Y.; Zeng, Y.; Lacey, S.D.; Li, Y.; Wang, Y.; Dai, J.; Wang, Y.; et al. Thermoelectric properties and performance of flexible reduced graphene oxide films up to 3000 K. *Nat. Energy* **2018**, *3*, 148–156. [[CrossRef](#)]
2. Hadjipanayis, G.C.; Gabay, A.M.; Schönhöbel, A.M.; Martín-Cid, A.; Barandiaran, J.M.; Niarchos, D. ThMn₁₂-Type Alloys for Permanent Magnets. *Engineering* **2020**, *6*, 141–147. [[CrossRef](#)]
3. Jacko, P.; Duranka, P.; Varga, R. Advantages of Bistable Microwires in Digital Signal Processing. *Sensors* **2024**, *24*, 2423. [[CrossRef](#)]
4. Mohri, K.; Uchiyama, T.; Panina, L.V.; Yamamoto, M.; Bushida, K. Recent Advances of Amorphous Wire CMOS IC Magneto-Impedance Sensors: Innovative High-Performance Micromagnetic Sensor Chip. *J. Sens.* **2015**, *2015*, 718069. [[CrossRef](#)]
5. Hasmonay, E.; Depeyrot, J.; Sousa, M.H.; Tourinho, F.A.; Bacri, J.C.; Perzynski, R.; Raikher, Y.L.; Rosenman, I. Magnetic and optical properties of ionic ferrofluids based on nickel ferrite nanoparticles. *J. Appl. Phys.* **2000**, *88*, 6628. [[CrossRef](#)]
6. Salaheldeen, M.; Zhukova, V.; Gonzalez, J.; Zhukov, A. The Effect of High-Temperature Annealing on the Magnetic and Structural Properties of (MnFePSi)-Based Glass-Coated Microwires. *Crystals* **2025**, *15*, 311. [[CrossRef](#)]
7. Al-Senani, G.M.; Al-Fawzan, F.F.; Almufarij, R.S.; Abd-Elkader, O.H.; Deraz, N.M. Magnetic Behavior of Virgin and Lithiated NiFe₂O₄ Nanoparticles. *Crystals* **2023**, *13*, 69. [[CrossRef](#)]
8. Salaheldeen, M.; Zhukova, V.; Rosero-Romo, J.J.; Ipatov, M.; Zhukov, A. Preparation and magnetic properties of MnFePSi-based glass-coated microwires. *AIP Adv.* **2024**, *14*, 015350. [[CrossRef](#)]
9. Hakim, M.L.; Alam, T.; Islam, M.S.; Salaheldeen, M.; Almalki, S.H.A.; Baharuddin, M.H.; Alsaif, H.; Islam, M.T. Wide-Oblique-Incident-Angle Stable Polarization-Insensitive Ultra-Wideband Metamaterial Perfect Absorber for Visible Optical Wavelength Applications. *Materials* **2022**, *15*, 2201. [[CrossRef](#)]
10. Liu, J.; Ma, W.-Z.; Chen, W.; Chen, Y.-S.; Deng, X.-C.; Gu, Y. A Metamaterial Absorber Based on Particle Swarm Optimization Suitable for Earth's Atmospheric Transparency Window. *IEEE Access* **2021**, *9*, 92941–92951. [[CrossRef](#)]
11. Parkin, S.; Yang, S.-H. Memory on the racetrack. *Nat. Nanotechnol.* **2015**, *10*, 195–198. [[CrossRef](#)] [[PubMed](#)]
12. Borders, W.A.; Pervaiz, A.Z.; Fukami, S.; Camsari, K.Y.; Ohno, H.; Datta, S. Integer factorization using stochastic magnetic tunnel junctions. *Nature* **2019**, *573*, 390–393. [[CrossRef](#)]
13. Shilkamy, H.A.E.-S.; Salaheldeen, M.; Zhukov, A.; El-Kasaby, R.A.; Feizi-Dehmayebi, M.; Alharas, M.M.A.; Abo-Dief, H.M.; El-Khatib, R.M.; Abu-Dief, A.M. Enhanced Corrosion Protection as a Sustainable Approach for Nickel Using Novel FeL Salen Complex: Electrochemical Investigation and DFT Insights. *Metals* **2025**, *15*, 403. [[CrossRef](#)]
14. Hoop, M.; Ribeiro, A.S.; Rösch, D.; Weinand, P.; Mendes, N.; Mushtaq, F.; Chen, X.Z.; Shen, Y.; Pujante, C.F.; Puigmartí-Luis, J.; et al. Mobile Magnetic Nanocatalysts for Bioorthogonal Targeted Cancer Therapy. *Adv. Funct. Mater.* **2018**, *28*, 1705920. [[CrossRef](#)]
15. Graf, T.; Parkin, S.S.P.; Felser, C. Heusler Compounds—A Material Class with Exceptional Properties. *IEEE Tran. Magn.* **2011**, *47*, 367–373. [[CrossRef](#)]
16. Karnaushenko, D.; Karnaushenko, D.D.; Makarov, D.; Baunack, S.; Schäfer, R.; Schmidt, O.G. Self-Assembled On-Chip-Integrated Giant Magneto-Impedance Sensorics. *Adv. Mater.* **2015**, *27*, 6582–6589. [[CrossRef](#)] [[PubMed](#)]
17. Gabay, A.M.; Hadjipanayis, G.C. Recent Developments in RFe₁₂-Type Compounds for Permanent Magnets. *Scr. Mater.* **2018**, *154*, 284–288. [[CrossRef](#)]
18. Alahmadi, M.; Mohamed, W.S.; Zhukov, A.; Salaheldeen, M.; Alsaedi, W.H.; Alhashmialameer, D.; Al-Ghamdi, K.; Abu Dief, A.M. One-step hydrothermal synthesis of flower-like MoS₂/VS₂ nanocomposite for biomedical applications. *Inorg. Chem. Commun.* **2023**, *157*, 111336. [[CrossRef](#)]
19. Khilwani, D.; Moghe, V.; Saraswat, V.; Kumbhare, P.; Baghini, M.J.; Jandhyala, S.; Subramoney, S.; Ganguly, U. Pr_xCa_{1-x}MnO₃ based neuron for Boltzmann machine to solve “maximum cut” problem. *APL Mater.* **2019**, *7*, 091112. [[CrossRef](#)]
20. Salaheldeen, M.; Mendez, M.; Vega, V.; Fernández, A.; Prida, V.M. Tuning Nanohole Sizes in Ni Hexagonal Antidot Arrays: Large Perpendicular Magnetic Anisotropy for Spintronic Applications. *ACS Appl. Nano Mater.* **2019**, *2*, 1866–1875. [[CrossRef](#)]
21. Musa, A.; Hakim, M.L.; Alam, T.; Islam, M.T.; Alshammari, A.S.; Mat, K.; M., M.S.; Almalki, S.H.A.; Islam, M.S. Polarization Independent Metamaterial Absorber with Anti-Reflection Coating Nanoarchitectonics for Visible and Infrared Window Applications. *Materials* **2022**, *15*, 3733. [[CrossRef](#)] [[PubMed](#)]
22. Salaheldeen, M.; Nafady, A.; Abu-Dief, A.M.; Díaz Crespo, R.; Fernández-García, M.P.; Andrés, J.P.; López Antón, R.; Blanco, J.A.; Álvarez-Alonso, P. Enhancement of Exchange Bias and Perpendicular Magnetic Anisotropy in CoO/Co Multilayer Thin Films by Tuning the Alumina Template Nanohole Size. *Nanomaterials* **2022**, *12*, 2544. [[CrossRef](#)] [[PubMed](#)]
23. Salaheldeen, M.; Vega, V.; Caballero-Flores, R.; Prida, V.M.; Fernández, A. Influence of nanoholes array geometrical parameters on magnetic properties of Dy-Fe antidot thin films. *Nanotechnology* **2019**, *30*, 455703. [[CrossRef](#)] [[PubMed](#)]
24. Skjærvø, S.H.; Marrows, C.H.; Stamps, R.L.; Heyderman, L.J. Advances in artificial spin ice. *Nat. Rev. Phys.* **2019**, *2*, 13–28. [[CrossRef](#)]
25. Salaheldeen, M.; Abu-Dief, A.M.; Martínez-Goyeneche, L.; Alzahrani, S.O.; Alkhatib, F.; Álvarez-Alonso, P.; Blanco, J.A. Dependence of the Magnetization Process on the Thickness of Fe₇₀Pd₃₀ Nanostructured Thin Film. *Materials*. **2020**, *13*, 5788. [[CrossRef](#)]

26. Maniv, E.; Murphy, R.A.; Haley, S.C.; Doyle, S.; John, C.; Maniv, A.; Ramakrishna, S.K.; Tang, Y.-L.; Ercius, P.; Ramesh, R.; et al. Exchange bias due to coupling between coexisting antiferromagnetic and spin-glass orders. *Nat. Phys.* **2021**, *17*, 525–530. [[CrossRef](#)]
27. Abu-Dief, A.M.; Salaheldeen, M.; El-Dabea, T. Recent advances in the development of gold nanoparticles for drug delivery systems. *J. Mod. Nanotechnol.* **2021**, *1*. [[CrossRef](#)]
28. Hirayama, Y.; Takahashi, Y.K.; Hirosawa, S.; Hono, K. Intrinsic Hard Magnetic Properties of $\text{Sm}(\text{Fe}_{1-x}\text{Co}_x)_{12}$ Compound with the ThMn_{12} Structure. *Scr. Mater.* **2017**, *138*, 62–65. [[CrossRef](#)]
29. Finocchio, G.; Bandyopadhyay, S.; Lin, P.; Pan, G.; Yang, J.J.; Tomasello, R.; Panagopoulos, C.; Carpentieri, M.; Puliafito, V.; Åkerman, J.; et al. Roadmap for unconventional computing with nanotechnology. *Nano Futures* **2024**, *8*, 012001. [[CrossRef](#)]
30. Prida, V.; Salaheldeen, M.; Pfitzer, G.; Hidalgo, A.; Vega, V.; González, S.; Teixeira, J.; Fernández, A.; Hernando, B. Template Assisted Deposition of Ferromagnetic Nanostructures: From Antidot Thin Films to Multisegmented Nanowires. *Acta Phys. Pol. A* **2017**, *131*, 822–827. [[CrossRef](#)]
31. Meiklejohn, W.H.; Bean, C.P. New Magnetic Anisotropy. *Phys. Rev.* **1957**, *105*, 904–913. [[CrossRef](#)]
32. Lukin, K.; Zemlyanyi, O.; Lukin, S. Generation of chaotic and random signals for noise radar-brief overview. In Proceedings of the 23rd International Radar Symposium (IRS), Gdansk, Poland, 12–14 September 2022.
33. Salaheldeen, M.; Zhukova, V.; Ipatov, M.; Zhukov, A. GdFe-based nanostructured thin films with large perpendicular magnetic anisotropy for spintronic applications. *AIP Adv.* **2024**, *14*, 025308. [[CrossRef](#)]
34. Yang, S.-H.; Ryu, K.-S.; Parkin, S. Domain-wall velocities of up to 750 m s^{-1} driven by exchange-coupling torque in synthetic antiferromagnets. *Nat. Nanotechnol.* **2015**, *10*, 221–226. [[CrossRef](#)]
35. Salaheldeen, M.; Goyeneche, M.L.M.; Alvarez-Alonso, P.; Fernandez, A. Enhancement the perpendicular magnetic anisotropy of nanopatterned hard/soft bilayer magnetic antidot arrays for spintronic application. *Nanotechnology* **2020**, *31*, 485708. [[CrossRef](#)]
36. Wolf, S.A.; Awschalom, D.D.; Buhrman, R.A.; Daughton, J.M.; von Molnár, S.; Roukes, M.L.; Chtchelkanova, A.Y.; Treger, D.M. Spintronics: A spin-based electronics vision for the future. *Science* **2001**, *294*, 1488–1495. [[CrossRef](#)]
37. Ali, M.M.K.; Ahmed, H.M.A.E.-L.; Salaheldeen, M.; Abu-Dief, A.M. Ultra-Density Nanostructure GdFe Thin Film with Large Perpendicular Magnetic Anisotropy for a New Generation of Spintronic Device. U.S. Patent 11,804,322 B1, 31 October 2023.
38. Tarnawski, J.; Buszman, K.; Woloszyn, M.; Puchalski, B. The Influence of the Geographic Positioning System Error on the Quality of Ship Magnetic Signature Reproduction Based on Measurements in Sea Conditions. *Measurement* **2024**, *229*, 114405. [[CrossRef](#)]
39. Moriya, R.; Hayashi, M.; Thomas, L.; Rettner, C.; Parkin, S.S.P. Dependence of field driven domain wall velocity on cross-sectional area in $\text{Ni}_{65}\text{Fe}_{20}\text{Co}_{15}$ nanowires. *Appl. Phys. Lett.* **2010**, *97*, 142506. [[CrossRef](#)]
40. Elphick, K.; Frost, W.; Samiepour, M.; Kubota, T.; Takanashi, K.; Sukegawa, H.; Mitani, S.; Hirohata, A. Heusler Alloys for Spintronic Devices: Review on Recent Development and Future Perspectives. *Sci. Technol. Adv. Mater.* **2021**, *22*, 235–271. [[CrossRef](#)]
41. Salaheldeen, M.; EskMnFeander, T.N.A.; Fathalla, M.; Zhukova, V.; Blanco, J.M.; Gonzalez, J.; Zhukov, A.; Abu-Dief, A.M. Empowering the Future: Cutting-Edge Developments in Supercapacitor Technology for Enhanced Energy Storage. *Batteries* **2025**, *11*, 232. [[CrossRef](#)]
42. Saccone, M.; Scholl, A.; Velten, S.; Dhuey, S.; Hofhuis, K.; Wuth, C.; Huang, Y.-L.; Chen, Z.; Chopdekar, R.V.; Farhan, A. Towards artificial Ising spin glasses: Thermal ordering in randomized arrays of Ising-type nanomagnets. *Phys. Rev. B* **2020**, *99*, 224403. [[CrossRef](#)]
43. Salaheldeen, M.; Vega, V.; Ibabe, A.; Jaafar, M.; Asenjo, A.; Fernandez, A.; Prida, V.M. Tailoring of Perpendicular Magnetic Anisotropy in $\text{Dy}_{13}\text{Fe}_{87}$ Thin Films with Hexagonal Antidot Lattice Nanostructure. *Nanomaterials* **2018**, *8*, 227. [[CrossRef](#)] [[PubMed](#)]
44. Salaheldeen, M.; Zhukova, V.; Gonzalez, J.; Zhukov, A. Grain Size Engineering and Tuning of Magnetic Properties in Ultra-Thin NiMnGa Glass-Coated Microwires: Insights from Annealing Effects. *Crystals* **2025**, *15*, 565. [[CrossRef](#)]
45. Nguyen, H.L.; Nam Nguyen, H.; Hai Nguyen, H.; Quynh Luu, M.; Hieu Nguyen, M. Nanoparticles: Synthesis and applications in life science and environmental technology. *Adv. Nat. Sci. Nanosci. Nanotechnol.* **2015**, *6*, 015008. [[CrossRef](#)]
46. Telegin, A.; Sukhorukov, Y. Magnetic Semiconductors as Materials for Spintronics. *Magnetochemistry* **2022**, *8*, 173. [[CrossRef](#)]
47. Barner, K. *New Trends in the Characterization of CMR-Manganites and Related Materials*; Research Signpost: Gottingen, Germany, 2005; p. 1.
48. Metawa, A.; El-Hossary, F.; Raaif, M.; SalahEl-Deen, M.; El-Moula, A.A.A. Langmuir probe and optical emission spectroscopy studies for RF magnetron sputtering during TiON thin film deposition. *Chin. J. Phys.* **2020**, *68*, 168–177. [[CrossRef](#)]
49. Telegin, A.V.; Sukhorukov, Y.P.; Loshkareva, N.N.; Mostovshchikova, E.V.; Bebenin, N.G.; Gan'shina, E.A.; Granovsky, A.B. Giant magnetotransmission and magnetoreflexion in ferromagnetic materials. *JMMM* **2015**, *383*, 104–109. [[CrossRef](#)]
50. Yamada, Y.; Ueno, K.; Fukumura, T.; Yuan, H.T.; Shimotani, H.; Iwasa, Y.; Kawasaki, M. Electrically induced ferromagnetism at room temperature in cobalt-doped titanium dioxide. *Science* **2011**, *332*, 1065–1067. [[CrossRef](#)] [[PubMed](#)]
51. Rizal, C.; Shimizu, H.; Mejia-Salazar, J.R. Magneto-Optics effects: New trends and future prospects for technological developments. *Magnetochemistry* **2022**, *8*, 94. [[CrossRef](#)]

52. Tavares, S.; Yang, K.; Meyers, M.A. Heusler alloys: Past, properties, new alloys, and prospects. *Prog. Mater. Sci.* **2023**, *132*, 101017. [[CrossRef](#)]
53. Voelkerding, K.V.; Dames, S.A.; Durtschi, J.D. Next-generation sequencing: From basic research to diagnostics. *Clin. Chem.* **2009**, *55*, 641–658. [[CrossRef](#)]
54. Salaheldeen, M.; Garcia-Gomez, A.; Corte-Leon, P.; Ipatov, M.; Zhukova, V.; Gonzalez, J.; Zhukov, A. Anomalous Magnetic Behavior in Half-Metallic Heusler Co₂FeSi Alloy Glass-Coated Microwires with High Curie Temperature. *J. Alloys Compd.* **2022**, *923*, 166379. [[CrossRef](#)]
55. Galanakis, I.; Dederichs, P.H.; Papanikolaou, N. Slater-Pauling Behavior and Origin of the Half-Metallicity of the Full-Heusler Alloys. *Phys. Rev. B* **2002**, *66*, 174429. [[CrossRef](#)]
56. Hazra, B.K.; Kaul, S.N.; Srinath, S.; Raja, M.M. Uniaxial Anisotropy, Intrinsic and Extrinsic Damping in Co₂FeSi Heusler Alloy Thin Films. *J. Phys. D Appl. Phys.* **2019**, *52*, 325002. [[CrossRef](#)]
57. Kojima, T.; Kameoka, S.; Tsai, A.-P. Heusler Alloys: A Group of Novel Catalysts. *ACS Omega* **2017**, *2*, 147–153. [[CrossRef](#)]
58. Graf, T.; Felser, C.; Parkin, S.S.P. Simple rules for the understanding of Heusler compounds. *Prog. Solid State Chem.* **2011**, *39*, 1. [[CrossRef](#)]
59. Ziebeck, K.R.A.; Neumann, K.-U. Magnetic Properties of metals. In *Landolt-Börnstein, New Series, Group III.*; Wijn, H.R.J., Ed.; Springer: Berlin/Heidelberg, Germany, 2001; Volume 32c, pp. 64–414.
60. Galanakis, I.; Özdoğan, K.; Şaşıoğlu, E. Spin-filter and spin-gapless semiconductors: The case of Heusler compounds. *AIP Adv.* **2016**, *6*, 055606. [[CrossRef](#)]
61. Gillessen, M.; Dronskowski, R. A combinatorial study of full Heusler alloys by first-principles computational methods. *J. Comput. Chem.* **2009**, *30*, 1290. [[CrossRef](#)]
62. Marathe, M.; Herper, H.C. Exploration of all-3d Heusler alloys for permanent magnets: An ab initio based high-throughput study. *Phys. Rev. B* **2023**, *107*, 174402. [[CrossRef](#)]
63. Nia, S.; Khenchoul, S.; Lefkaier, I.K.; Lagoun, B. DFT-based investigation of the structural, magnetic, electronic, half-metallicity and elastic properties in the all-d heusler compounds: The case of Co₂VZn and CoVZn. *Eur. Phys. J. B* **2021**, *94*, 118. [[CrossRef](#)]
64. Wurmehl, S.; Fecher, G.H.; Kandpal, H.C.; Ksenofontov, V.; Felser, C.; Lin, H.J.; Morais, J. Geometric, Electronic, and Magnetic Structure of Co₂FeSi: Curie Temperature and Magnetic Moment Measurements and Calculations. *Phys. Rev. B Condens. Matter. Mater. Phys.* **2005**, *72*, 184434. [[CrossRef](#)]
65. Isa, M.C.; Nain, H.; Yusoff, N.H.N.; Manap, A.R.A.; Slamatt, R.; Anuar, M.H. An Overview of Ship Magnetic Signature and Silencing Technologies. *Def. ST Tech. Bull.* **2019**, *12*, 176–192.
66. Salaheldeen, M.; Garcia-Gomez, A.; Ipatov, M.; Corte-Leon, P.; Zhukova, V.; Blanco, J.M.; Zhukov, A. Fabrication and Magneto-Structural Properties of Co₂-Based Heusler Alloy Glass-Coated Microwires with High Curie Temperature. *Chemosensors* **2022**, *10*, 225. [[CrossRef](#)]
67. Tarnawski, J.; Buszman, K.; Woloszyn, M.; Rutkowski, T.A.; Cichocki, A.; Józwiak, R. Measurement Campaign and Mathematical Model Construction for the Ship Zodiak Magnetic Signature Reproduction. *Measurement* **2021**, *186*, 110059. [[CrossRef](#)]
68. Abdul Rauf, A.M.; Mohd Hambali, A.; Mahdi Che, I.; Mohd Hazri, R.; Roslan, S.; Mohd Yusri, O.; Hasril, N.; Zuraini, A.M.; Muhammad Syauqat, A.K. Magnetic Assessment of Newly Installed Onboard Degaussing System. *Def. ST Tech. Bull.* **2018**, *11*, 265–276.
69. Li, P.; Koo, J.; Ning, W.; Li, J.; Miao, L.; Min, L.; Zhu, Y.; Wang, Y.; Alem, N.; Liu, C.X.; et al. Giant Room Temperature Anomalous Hall Effect and Tunable Topology in a Ferromagnetic Topological Semimetal Co₂MnAl. *Nat. Commun.* **2020**, *11*, 3476. [[CrossRef](#)]
70. Belopolski, I.; Manna, K.; Sanchez, D.S.; Chang, G.; Ernst, B.; Yin, J.; Zhang, S.S.; Cochran, T.; Shumiya, N.; Zheng, H.; et al. Discovery of Topological Weyl Fermion Lines and Drumhead Surface States in a Room Temperature Magnet. *Science* **2019**, *365*, 1278–1281. [[CrossRef](#)]
71. Guillemard, C.; Petit-Watelot, S.; Pasquier, L.; Pierre, D.; Ghanbaja, J.; RojasSánchez, J.C.; Bataille, A.; Rault, J.; le Fèvre, P.; Bertran, F.; et al. Ultralow Magnetic Damping in Co₂Mn-Based Heusler Compounds: Promising Materials for Spintronics. *Phys. Rev. Appl.* **2019**, *11*, 064009. [[CrossRef](#)]
72. Hirohata, A.; Sagar, J.; Lari, L.; Fleet, L.R.; Lazarov, V.K. Heusler-alloy films for spintronic devices. *Appl. Phys. A* **2013**, *111*, 423–430. [[CrossRef](#)]
73. Jourdan, M.; Minár, J.; Braun, J.; Kronenberg, A.; Chadov, S.; Balke, B.; Gloskovskii, A.; Kolbe, M.; Elmers, H.J.; Schönhense, G.; et al. Direct Observation of Half-Metallicity in the Heusler Compound Co₂MnSi. *Nat. Commun.* **2014**, *5*, 3974. [[CrossRef](#)]
74. Patra, N.; Prajapat, C.L.; Babu, P.D.; Rai, S.; Kumar, S.; Jha, S.N.; Bhattacharyya, D. Pulsed Laser Deposited Co₂FeSi Heusler Alloy Thin Films: Effect of Different Thermal Growth Processes. *J. Alloys Compd.* **2019**, *804*, 470–485. [[CrossRef](#)]
75. Salaheldeen, M.; Ipatov, M.; Zhukova, V.; García-Gomez, A.; Gonzalez, J.; Zhukov, A. Preparation and magnetic properties of Co₂-based Heusler alloy glass-coated microwires with high Curie temperature. *AIP Adv.* **2023**, *13*, 025325. [[CrossRef](#)]
76. Sapkota, K.R.; Gyawali, P.; Forbes, A.; Pegg, I.L.; Philip, J. Synthesis and Characterization of Co₂FeAl Nanowires. *J. Appl. Phys.* **2012**, *111*, 123906. [[CrossRef](#)]

77. Simon, P.; Wolf, D.; Wang, C.; Levin, A.A.; Lubk, A.; Sturm, S.; Lichte, H.; Fecher, G.H.; Felser, C. Synthesis and Three-Dimensional Magnetic Field Mapping of Co₂FeGa Heusler Nanowires at 5 Nm Resolution. *Nano Lett.* **2016**, *16*, 114–120. [[CrossRef](#)] [[PubMed](#)]
78. Salaheldeen, M.; Garcia, A.; Corte-Leon, P.; Ipatov, M.; Zhukova, V.; Zhukov, A. Unveiling the Effect of Annealing on Magnetic Properties of Nanocrystalline Half-Metallic Heusler Co₂FeSi Alloy Glass-Coated Microwires. *J. Mater. Res. Technol.* **2022**, *20*, 4161–4172. [[CrossRef](#)]
79. Li, W.J.; Khan, U.; Irfan, M.; Javed, K.; Liu, P.; Ban, S.L.; Han, X.F. Fabrication and Magnetic Investigations of Highly Uniform CoNiGa Alloy Nanowires. *J. Magn. Magn. Mater.* **2017**, *432*, 124–128. [[CrossRef](#)]
80. Salaheldeen, M.; Ipatov, M.; Corte-Leon, P.; Zhukova, V.; Zhukov, A. Effect of Annealing on the Magnetic Properties of Co₂MnSi-Based Heusler Alloy Glass-Coated Microwires. *Metals* **2023**, *13*, 412. [[CrossRef](#)]
81. Khovaylo, V.V.; Rodionova, V.V.; Shevyrtalov, S.N.; Novosad, V. Magnetocaloric Effect in “Reduced” Dimensions: Thin Films, Ribbons, and Microwires of Heusler Alloys and Related Compounds. *Phys. Status Solidi* **2014**, *251*, 2104–2113. [[CrossRef](#)]
82. Belmeguenai, M.; Tuzcuoglu, H.; Gabor, M.S.; Petrisor, T.; Tiusan, C.; Zighem, F.; Chérif, S.M.; Moch, P. Co₂FeAl Heusler Thin Films Grown on Si and MgO Substrates: Annealing Temperature Effect. *J. Appl. Phys.* **2014**, *115*, 043918. [[CrossRef](#)]
83. Bai, Z.; Shen, L.E.I.; Han, G.; Feng, Y.P. Data Storage: Review of Heusler Compounds. *Spin* **2012**, *2*, 1230006. [[CrossRef](#)]
84. Herzer, G. Modern soft magnets: Amorphous and nanocrystalline materials. *Acta Mater.* **2013**, *61*, 718–734. [[CrossRef](#)]
85. Klement, K.; Wilens, R.H.; Duwez, P. Non-crystalline structure in solidified Gold-Silicon alloys. *Nature* **1970**, *187*, 869–870. [[CrossRef](#)]
86. Wilson, S.A.; Jourdain, R.P.J.; Zhang, Q.; Dorey, R.A.; Bowen, C.R.; Willander, M.; Wahab, Q.U.; Willander, M.; Al-hilli, S.M.; Nur, O.; et al. New materials for micro-scale sensors and actuators: An engineering review. *Mater. Sci. Eng. R-Rep.* **2007**, *56*, 1–129. [[CrossRef](#)]
87. Salaheldeen, M.; Zhukova, V.; Gonzalez, J.; Zhukov, A. Anomalous magnetic behavior in MnFePSi glass-coated microwires. *J. Alloys Compd.* **2024**, *1002*, 175244. [[CrossRef](#)]
88. Zhukov, A.; Rodionova, V.; Ilyn, M.; Aliev, A.M.; Varga, R.; Michalik, S.; Aronin, A.; Abrosimova, G.; Kiselev, A.; Ipatov, M.; et al. Magnetic properties and magnetocaloric effect in Heusler-type glass-coated NiMnGa microwires. *J. Alloys Compd.* **2013**, *575*, 73–79. [[CrossRef](#)]
89. Zhukova, V.; Corte-Leon, P.; Blanco, J.M.; Ipatov, M.; Gonzalez-Legarreta, L.; Gonzalez, A.; Zhukov, A. Development of Magnetically Soft Amorphous Microwires for Technological Applications. *Chemosensors* **2022**, *10*, 26. [[CrossRef](#)]
90. McHenry, M.; Willard, M.; Laughlin, D. Amorphous and Nanocrystalline Materials for Applications as Soft Magnets. *Prog. Mater. Sci.* **1999**, *44*, 291. [[CrossRef](#)]
91. Masumoto, T.; Hashimoto, K. Corrosion properties of amorphous metals. *J. Phys. Colloq.* **1980**, *41*, C8-894–C8-900. [[CrossRef](#)]
92. Salaheldeen, M.; Zhukova, V.; Lopez Anton, R.; Zhukov, A. Dependence of Magnetic Properties of As-Prepared Nanocrystalline Ni₂MnGa Glass-Coated Microwires on the Geometrical Aspect Ratio. *Sensors* **2024**, *24*, 3692. [[CrossRef](#)]
93. Zhukov, A.; Corte-Leon, P.; Gonzalez-Legarreta, L.; Ipatov, M.; Blanco, J.M.; Gonzalez, A.; Zhukova, V. Advanced functional magnetic microwires for technological applications. *J. Phys. D Appl. Phys.* **2022**, *55*, 253003. [[CrossRef](#)]
94. Qin, F.; Peng, H.X. Ferromagnetic microwires enabled multifunctional composite materials. *Prog. Mater. Sci.* **2013**, *58*, 183–259. [[CrossRef](#)]
95. Chiriac, H.; Óvári, T.A.; Pop, G. Internal stress distribution in glass-covered amorphous magnetic wires. *Phys. Rev. B* **1995**, *52*, 10104–10113. [[CrossRef](#)] [[PubMed](#)]
96. Goto, T. Fe-B and Fe-Si-B system alloy filaments produced by glass-coated melt spinning. *Trans. JIM* **1980**, *21*, 219–224. [[CrossRef](#)]
97. Schuh, C.A.; Hufnagel, T.C.; Ramamurty, U. Mechanical behavior of amorphous alloys. *Acta Mater.* **2007**, *55*, 4067–4109. [[CrossRef](#)]
98. Hagiwara, M.; Inoue, A.; Masumoto, T. Mechanical properties of Fe–Si–B amorphous wires produced by in-rotating-water spinning method. *Metall. Trans. A* **1982**, *13*, 373–382. [[CrossRef](#)]
99. Goto, T.; Nagano, M.; Wehara, N. Mechanical properties of amorphous Fe₈₀P₁₆C₃B₁ filament produced by glass-coated melt spinning. *Trans. JIM* **1977**, *18*, 759–764. [[CrossRef](#)]
100. Baranov, S.A.; Larin, V.S.; Torcunov, A.V. Technology, Preparation and Properties of the Cast Glass-Coated Magnetic Microwires. *Crystals* **2017**, *7*, 136. [[CrossRef](#)]
101. Kozejova, D.; Fecova, L.; Klein, P.; Sabol, R.; Hudak, R.; Sulla, I.; Mudronova, D.; Galik, J.; Varga, R. Biomedical Applications of Glass-Coated Microwires. *J. Magn. Magn. Mater.* **2019**, *470*, 2–5. [[CrossRef](#)]
102. Ulitovsky, A.V.; Maianski, I.M.; Avramenco, A.I. 1960 Method of Continuous Casting of Glass Coated Microwire. USSR Patent 128427, 6 May 1960.
103. Salaheldeen, M.; Garcia-Gomez, A.; Corte-León, P.; Gonzalez, A.; Ipatov, M.; Zhukova, V.; Gonzalez, J.M.; López Antón, R.; Zhukov, A. Manipulation of Magnetic and Structure Properties of Ni₂FeSi Glass-Coated Microwires by Annealing. *J. Alloys Compd.* **2023**, *942*, 169026. [[CrossRef](#)]
104. Uddin, A.; Estevez, D.; Qin, F.X. From functional units to material design: A review on recent advancement of programmable microwire metacomposites. *Compos. Part A Appl. Sci. Manuf.* **2022**, *153*, 106734. [[CrossRef](#)]

105. Salaheldeen, M.; Wederni, A.; Ipatov, M.; Gonzalez, J.; Zhukova, V.; Zhukov, A. Elucidation of the Strong Effect of the Annealing and the Magnetic Field on the Magnetic Properties of Ni₂-Based Heusler Microwires. *Crystals* **2022**, *12*, 1755. [[CrossRef](#)]
106. Salaheldeen, M.; Wederni, A.; Ipatov, M.; Zhukova, V.; Lopez Anton, R.; Zhukov, A. Enhancing the Squareness and Bi-Phase Magnetic Switching of Co₂FeSi Microwires for Sensing Application. *Sensors* **2023**, *23*, 5109. [[CrossRef](#)] [[PubMed](#)]
107. Hennel, M.; Varga, M.; Frolova, L.; Nalevanko, S.; Ibarra-Gaytán, P.; Vidyasagar, R.; Sarkar, P.; Dzubinska, A.; Galdun, L.; Ryba, T.; et al. Heusler-Based Cylindrical Micro- and Nanowires. *Phys. Status Solidi A* **2022**, *219*, 2100657. [[CrossRef](#)]
108. Salaheldeen, M.; Zhukova, V.; Zhukov, A. Unraveling the impact of annealing and magnetic field on MnFePSi microwires. *J. Appl. Phys.* **2024**, *136*, 133902. [[CrossRef](#)]
109. Chiriac, H.; Lupu, N.; Stoian, G.; Ababei, G.; Corodeanu, S.; Óvári, T.A. Ultrathin Nanocrystalline Magnetic Wires. *Crystals* **2017**, *7*, 48. [[CrossRef](#)]
110. Chiriac, H.; Ovari, T.-A. Amorphous glass-covered magnetic wires: Preparation, properties, applications. *Prog. Mater. Sci.* **1996**, *40*, 333–407. [[CrossRef](#)]
111. Alam, J.; Nematov, M.; Yudanov, N.; Podgornaya, S.; Panina, L. High-Frequency Magnetoimpedance (MI) and Stress-MI in Amorphous Microwires with Different Anisotropies. *Nanomaterials* **2021**, *11*, 1208. [[CrossRef](#)] [[PubMed](#)]
112. Klein, P.; Varga, R.; Badini-Confalonieri, G.A.; Vazquez, M. Domain Wall Dynamics in Amorphous and Nanocrystalline FeCoMoB Microwires. *J. Nanosci. Nanotechnol.* **2012**, *12*, 7464–7467. [[CrossRef](#)]
113. Torcunov, A.V.; Baranov, S.A.; Larin, V.S. The internal stresses dependence of the magnetic properties of cast amorphous microwires covered with glass insulation. *J. Magn. Magn. Mater.* **1999**, *196–197*, 835–836. [[CrossRef](#)]
114. Corodeanu, S.; Hlenschi, C.; Chiriac, H.; Óvári, T.-A.; Lupu, N. Comparative Study of the Magnetic Behavior of FINEMET Thin Magnetic Wires: Glass-Coated, Glass-Removed, and Cold-Drawn. *Materials* **2023**, *16*, 1340. [[CrossRef](#)]
115. Qin, F.; Peng, H.-X.; Tang, J.; Qin, L.-C. Ferromagnetic microwires enabled polymer composites for sensing applications. *Compos. Part A Appl. Sci. Manuf.* **2010**, *41*, 1823–1828. [[CrossRef](#)]
116. Nematov, M.G.; Baraban, I.; Yudanov, N.A.; Rodionova, V.; Qin, F.X.; Peng, H.X.; Panina, L.V. Evolution of the magnetic anisotropy and magnetostriction in Co-based amorphous alloys microwires due to current annealing and stress-sensory applications. *J. Alloys Compd.* **2020**, *837*, 155584. [[CrossRef](#)]
117. Mitxelena-Iribarren, O.; Campisi, J.; de Apellániz, I.M.; Lizarbe-Sancha, S.; Arana, S.; Zhukova, V.; Mujika, M.; Zhukov, A. Glass-coated ferromagnetic microwire-induced magnetic hyperthermia for in vitro cancer cell treatment. *Mater. Sci. Eng. C* **2020**, *106*, 110261. [[CrossRef](#)] [[PubMed](#)]
118. Herrero-Gómez, C.; Aragon, A.M.; Hernando-Rydings, M.; Marin, P.; Hernando, A. Stress and field contactless sensor based on the scattering of electromagnetic waves by a single ferromagnetic microwire. *Appl. Phys. Lett.* **2014**, *105*, 92405. [[CrossRef](#)]
119. Kostitsyna, E.V.; Gudoshnikov, S.A.; Popova, A.V.; Petrzhik, M.I.; Tarasov, V.P.; Usov, N.A.; Ignatov, A.S. Mechanical properties and internal quenching stresses in Co-rich amorphous ferromagnetic microwires. *J. Alloys Compd.* **2017**, *707*, 199–204. [[CrossRef](#)]
120. Dzhumazoda, A.; Panina, L.V.; Nematov, M.G.; Ukhasov, A.A.; Yudanov, N.A.; Morchenko, A.T.; Qin, F.X. Temperature-stable magnetoimpedance (MI) of current-annealed Co-based amorphous microwires. *J. Magn. Magn. Mater.* **2019**, *474*, 374–380. [[CrossRef](#)]
121. Astefanoaei, I.; Radu, D.; Chiriac, H. Internal stress distribution in DC joule-heated amorphous glass-covered microwires. *J. Condens. Matter. Phys.* **2006**, *18*, 2689–2716. [[CrossRef](#)]
122. Orlova, N.N.; Gornakov, V.S.; Aronin, A.S. Role of internal stresses in the formation of magnetic structure and magnetic properties of iron-based glass coated microwires. *J. Appl. Phys.* **2017**, *121*, 205108. [[CrossRef](#)]
123. Antonov, A.S.; Borisov, V.T.; Borisov, O.V.; Prokoshin, A.F.; Usov, N.A. Residual quenching stresses in glass-coated amorphous ferromagnetic microwires. *J. Phys. D Appl. Phys.* **2000**, *33*, 1161–1168. [[CrossRef](#)]
124. Chiriac, H.; Óvári, T.-A.; Corodeanu, S.; Ababei, G. Interdomain wall in amorphous glass-coated microwires. *Phys. Rev. B* **2007**, *76*, 214433. [[CrossRef](#)]
125. Panina, L.V.; Dzhumazoda, A.; Evstigneeva, S.A.; Adam, A.M.; Morchenko, A.T.; Yudanov, N.A.; Kostishyn, V.G. Temperature effects on magnetization processes and magnetoimpedance in low magnetostrictive amorphous microwires. *J. Magn. Magn. Mater.* **2018**, *459*, 147–153. [[CrossRef](#)]
126. Salaheldeen, M.; Zhukova, V.; Ipatov, M.; Zhukov, A. Unveiling the Magnetic and Structural Properties of (X₂YZ; X = Co and Ni, Y = Fe and Mn, and Z = Si) Full-Heusler Alloy Microwires with Fixed Geometrical Parameters. *Crystals* **2023**, *13*, 1550. [[CrossRef](#)]
127. Sigoli, F.A.; Kawano, Y.; Davolos, M.R.; Jafellicci, M., Jr. Phase separation in pyrex glass by hydrothermal treatment: Evidence from micro-Raman spectroscopy. *J. Non-Cryst. Solids* **2001**, *284*, 49–54. [[CrossRef](#)]
128. Cerqueira, M.F.; Andritschky, M.; Rebouta, L.; Ferreira, J.A.; da Silva, M.F. Macrocrystalline silicon thin films prepared by RF reactive magnetron sputter deposition. *Vacuum* **1995**, *46*, 1385–1390. [[CrossRef](#)]
129. Patra, N.; Prajapat, C.L.; Babu, P.D.; Rai, S.; Kumar, S.; Jha, S.N.; Bhattacharyya, D. Effect of growth temperature on the structural and magnetic properties of the pulsed laser deposited Co₂FeAl thin films. *J. Alloys Compd.* **2019**, *779*, 648–659. [[CrossRef](#)]

130. Demidov, E.S.; Sdobnyakov, V.V.; Vazenmiller, G.V.; Chigirinskii, Y.I.; Dudin, Y.A.; Lesnikov, V.P.; Trushin, V.N.; Boldin, M.S.; Belkin, O.A.; Bobrov, A.A.; et al. Manufacturing of sputtering composite targets containing phases of Co_2FeSi or Co_2MnSi Heusler alloy. *Tech. Phys.* **2018**, *63*, 1002–1005. [[CrossRef](#)]
131. Zhukova, V.; Cobeño, A.F.; Zhukov, A.; Blanco, J.M.; Larin, V.; Gonzalez, J. Coercivity of glass-coated $\text{Fe}_{73.4-x}\text{Cu}_1\text{Nb}_{3.1}\text{Si}_{13.4+x}\text{B}_{9.1}$ ($0 \leq x \leq 1.6$) microwires. *Nanostruct. Mater.* **1999**, *11*, 1319–1327. [[CrossRef](#)]
132. Herzer, G. Grain size dependence of coercivity and permeability in nanocrystalline ferromagnets. *IEEE Trans. Magn.* **1990**, *26*, 1397–1402. [[CrossRef](#)]
133. Kulik, T. Nanocrystallization of metallic glasses. *J. Non-Cryst. Solids* **2001**, *287*, 145–161. [[CrossRef](#)]
134. Greer, A.L. Crystallization of amorphous alloys. *Metall. Mater. Trans. A* **1996**, *27*, 549–555. [[CrossRef](#)]
135. Nabias, J.; Asfour, A.; Yonnet, J. Temperature Dependence of Giant Magnetoimpedance in Amorphous Microwires for Sensor Application. *IEEE Trans. Magn.* **2017**, *53*, 4001005. [[CrossRef](#)]
136. Wurmehl, S.; Fecher, G.H.; Ksenofontov, V.; Casper, F.; Stumm, U.; Felser, C.; Lin, H.J.; Hwu, Y. Half-Metallic Ferromagnetism with High Magnetic Moment and High Curie Temperature in Co_2FeSi . *J. Appl. Phys.* **2006**, *99*, 08J103. [[CrossRef](#)]
137. Boehnke, A.; Martens, U.; Sterwerf, C.; Niesen, A.; Huebner, T.; Von Der Ehe, M.; Meinert, M.; Kuschel, T.; Thomas, A.; Heiliger, C.; et al. Large Magneto-Seebeck Effect in Magnetic Tunnel Junctions with Half-Metallic Heusler Electrodes. *Nat. Commun.* **2017**, *8*, 1626. [[CrossRef](#)] [[PubMed](#)]
138. Buznikov, N.A.; Popov, V.V. A core-shell model for magnetoimpedance in stress-annealed Fe-rich amorphous microwires. *J. Supercond. Nov. Magn.* **2021**, *34*, 169–177. [[CrossRef](#)]
139. Guo, X.B.; Zuo, Y.L.; Cui, B.S.; Li, D.; Yun, J.J.; Wu, K.; Wang, T.; Xi, L. Post annealing induced magnetic anisotropy in CoFeSi thin films on $\text{MgO}(001)$. *J. Phys. D Appl. Phys.* **2017**, *50*, 085006. [[CrossRef](#)]
140. Óvári, T.-A.; Lupu, N.; Chiriac, H. Rapidly Solidified Magnetic Nanowires and Submicron Wires. In *Advanced Magnetic Materials*; Malkinski, L., Ed.; InTech: London, UK, 2012; pp. 1–32. ISBN 978-953-51-0637-1.
141. Zhang, M.; Qu, G.; Liu, J.; Pang, M.; Wang, X.; Liu, R.; Cao, G.; Ma, G. Enhancement of Magnetic and Tensile Mechanical Performances in Fe-Based Metallic Microwires Induced by Trace Ni-Doping. *Materials* **2021**, *14*, 3589. [[CrossRef](#)]
142. Srinivas, K.; Manivel Raja, M.; Sridhara Rao, D.V.; Kamat, S.V. Effect of Sputtering Pressure and Power on Composition, Surface Roughness, Microstructure and Magnetic Properties of as-Deposited Co_2FeSi Thin Films. *Thin Solid Film.* **2014**, *558*, 349–355. [[CrossRef](#)]
143. Gunnarsson, K.; Svedlindh, P.; Andersson, J.O.; Nordblad, P.; Lundgren, L.; Aruga Katori, H.; Ito, A. Magnetic Behavior of a Reentrant Ising Spin Glass. *Phys. Rev. B* **1992**, *46*, 8227–8231. [[CrossRef](#)]
144. Rodionova, V.; Ipatov, M.; Ilyn, M.; Zhukova, V.; Perov, N.; Gonzalez, J.; Zhukov, A. Design of magnetic properties of arrays of magnetostatically coupled glass-covered magnetic microwires. *Phys. Status Solidi Appl. Mater. Sci.* **2010**, *207*, 1954–1959. [[CrossRef](#)]
145. Vazquez, M.; Gomez-Polo, C.; Chen, D.-X.; Hemando, A. Magnetic Bistability of Amorphous Wires and Sensor Applications. *IEEE Trans. Magn.* **1994**, *39*, 907–912. [[CrossRef](#)]
146. Kronmüller, H. Theory of the coercive field in amorphous ferromagnetic alloys. *J. Magn. Magn. Mater* **1981**, *24*, 159–167. [[CrossRef](#)]
147. Salaheldeen, M.; Zhukova, V.; Blanco, J.M.; Gonzalez, J.; Zhukov, A. The Impact of High-Temperature Annealing on Magnetic Properties, Structure and Martensitic Transformation of Ni_2MnGa -based Glass-Coated Microwires. *Ceram. Int.* **2024**, *51*, 4378–4387. [[CrossRef](#)]
148. Salaheldeen, M.; Talaat, A.; Ipatov, M.; Zhukova, V.; Zhukov, A. Preparation and Magneto-Structural Investigation of Nanocrystalline CoMn -Based Heusler Alloy Glass-Coated Microwires. *Processes* **2022**, *10*, 2248. [[CrossRef](#)]
149. Salaheldeen, M.; Wederni, A.; Ipatov, M.; Zhukova, V.; Zhukov, A. Preparation and Magneto-Structural Investigation of High Ordered ($L2_1$ Structure) Co_2MnGe Microwires. *Processes* **2023**, *11*, 1138. [[CrossRef](#)]
150. Rodionova, V.; Ipatov, M.; Ilyn, M.; Zhukova, V.; Perov, N.; Gonzalez, J.; Zhukov, A. Tailoring of Magnetic Properties of Magnetostatically-Coupled Glass-Covered Magnetic Microwires. *J Supercond Nov. Magn.* **2011**, *24*, 541–547. [[CrossRef](#)]
151. Zagrebin, M.A.; Sokolovskiy, V.V.; Buchelnikov, V.D. Electronic and magnetic properties of the Co_2 -based Heusler compounds under pressure: First-principles and Monte Carlo studies. *J. Phys. D Appl. Phys.* **2016**, *49*, 355004. [[CrossRef](#)]
152. Chernenko, V.A.; L'vov, V.A.; Zagorodnyuk, S.P.; Takagi, T. Ferromagnetism of thermoelastic martensites: Theory and experiment. *Phys. Rev. B* **2003**, *67*, 064407. [[CrossRef](#)]
153. Wederni, A.; Salaheldeen, M.; Ipatov, M.; Zhukova, V.; Zhukov, A. Influence of the Geometrical Aspect Ratio on the Magneto-Structural Properties of Co_2MnSi Microwires. *Metals* **2023**, *13*, 1692. [[CrossRef](#)]
154. Kubota, T.; Ina, Y.; Wen, Z.; Takanashi, K. Interface Tailoring Effect for Heusler Based CPP-GMR with an $L1_2$ -Type Ag_3Mg Spacer. *Materials* **2018**, *11*, 219. [[CrossRef](#)]
155. Kieven, D.; Klenk, R.; Naghavi, S.; Felser, C.; Gruhn, T. I-II-V half-Heusler compounds for optoelectronics: Ab initio calculations. *Phys. Rev.* **2010**, *B81*, 075208. [[CrossRef](#)]
156. Uto, O.T.; Adebambo, P.O.; Akinlami, J.O.; Kenmoe, S.; Adebayo, G.A. Electronic, Structural, Mechanical, and Thermodynamic Properties of CoYSb ($Y = \text{Cr, Mo, W}$) Half-Heusler Compounds as Potential Spintronic Materials. *Solids* **2022**, *3*, 22–33. [[CrossRef](#)]

157. Faleev, S.V.; Ferrante, Y.; Jeong, J.; Samant, M.G.; Jones, B.; Parkin, S.S.P. Origin of the tetragonal ground state of Heusler compounds. *Phys. Rev. Appl.* **2017**, *7*, 034022. [[CrossRef](#)]
158. Munir, J.; Jamil, M.; Jbara, A.S.; Fatima, K.; Ain, Q.; Ullah, H.; Yousaf, M. Spin-Polarized Electromagnetic and Optical Response of Full-Heusler Co_2VZ ($Z = \text{Al, Be}$) Alloys for Spintronic Application. *Eur. Phys. J. Plus* **2021**, *136*, 1009. [[CrossRef](#)]
159. Nawa, K.; Kurniawan, I.; Masuda, K.; Miura, Y.; Patrick, C.E.; Staunton, J.B. Temperature-Dependent Spin Polarization of Heusler Co_2MnSi from the Disordered Local-Moment Approach: Effects of Atomic Disordering and Nonstoichiometry. *Phys. Rev. B* **2020**, *102*, 054424. [[CrossRef](#)]
160. Kämmerer, S.; Thomas, A.; Hütten, A.; Reiss, G. Co_2MnSi Heusler alloy as magnetic electrodes in magnetic tunnel junctions. *Appl. Phys. Lett.* **2004**, *85*, 79. [[CrossRef](#)]
161. Wang, C.; Meyer, J.; Teichert, N.; Auge, A.; Rausch, E.; Balke, B.; Hütten, A.; Fecher, G.H.; Felser, C. Heusler Nanoparticles for Spintronics and Ferromagnetic Shape Memory Alloys. *J. Vac. Sci. Technol. B* **2014**, *32*, 020802. [[CrossRef](#)]
162. Aoki, M.; Yin, Y.; Granville, S.; Zhang, Y.; Medhekar, N.V.; Leiva, L.; Ohshima, R.; Ando, Y.; Shiraishi, M. Gigantic Anisotropy of Self-Induced Spin-Orbit Torque in Weyl Ferromagnet Co_2MnGa . *Nano Lett.* **2023**, *23*, 6951–6957. [[CrossRef](#)]
163. Ren, L.; Liu, L.; Song, X.; Zhao, T.; Xing, X.; Feng, Y.P.; Chen, J.; Teo, K.L. Manipulation of the Topological Ferromagnetic State in a Weyl Semimetal by Spin–Orbit Torque. *Nano Lett.* **2023**, *23*, 3394–3400. [[CrossRef](#)]
164. Ikeda, S.; Hayakawa, J.; Ashizawa, Y.; Lee, Y.M.; Miura, K.; Hasegawa, H.; Tsunoda, M.; Matsukura, F.; Ohno, H. Tunnel magnetoresistance of 604% at 300K by suppression of Ta diffusion in $\text{CoFeB}/\text{MgO}/\text{CoFeB}$ pseudo-spin-valves annealed at high temperature. *Appl. Phys. Lett.* **2008**, *93*, 082508. [[CrossRef](#)]
165. Tezuka, N.; Ikeda, N.; Mitsuhashi, F.; Sugimoto, S. Improved tunnel magnetoresistance of magnetic tunnel junctions with Heusler $\text{Co}_2\text{FeAl}_{0.5}\text{Si}_{0.5}$ electrodes fabricated by molecular beam epitaxy. *Appl. Phys. Lett.* **2009**, *94*, 162504. [[CrossRef](#)]
166. Mahendra, A.; Murmu, P.P.; Acharya, S.K.; Islam, A.; Fiedler, H.; Gupta, P.; Granville, S.; Kennedy, J. Shaping Perpendicular Magnetic Anisotropy of Co_2MnGa Heusler Alloy Using Ion Irradiation for Magnetic Sensor Applications. *Sensors* **2023**, *23*, 4564. [[CrossRef](#)]
167. Morón, C.; Cabrera, C.; Morón, A.; García, A.; González, M. Magnetic Sensors Based on Amorphous Ferromagnetic Materials: A Review. *Sensors* **2015**, *15*, 28340–28366. [[CrossRef](#)] [[PubMed](#)]
168. Khan, M.A.; Sun, J.; Li, B.; Przybysz, A.; Kosel, J. Magnetic Sensors—A Review and Recent Technologies. *Eng. Res. Express* **2021**, *3*, 022005. [[CrossRef](#)]
169. Mahendra, A.; Gupta, P.; Granville, S.; Kennedy, J. Tailoring of Magnetic Anisotropy by Ion Irradiation for Magnetic Tunnel Junction Sensors. *J. Alloys Compd.* **2022**, *910*, 164902. [[CrossRef](#)]
170. Kappe, D.; Bondzio, L.; Swager, J.; Becker, A.; Büker, B.; Ennen, I.; Schröder, C.; Hütten, A. Reviewing Magnetic Particle Preparation: Exploring the Viability in Biosensing. *Sensors* **2020**, *20*, 4596. [[CrossRef](#)] [[PubMed](#)]

Disclaimer/Publisher’s Note: The statements, opinions and data contained in all publications are solely those of the individual author(s) and contributor(s) and not of MDPI and/or the editor(s). MDPI and/or the editor(s) disclaim responsibility for any injury to people or property resulting from any ideas, methods, instructions or products referred to in the content.